Dilepton production in heavy-ion collisions at intermediate energies

K. Shekhter,[1] C. Fuchs,[1] Amand Faessler,[1] M. Krivoruchenko,[1,2] and B. Martemyanov[1,2]

[1]*Institut für Theoretische Physik der Universität Tübingen, Auf der Morgenstelle 14, D-72076 Tübingen, Germany*

[2]*Institute for Theoretical and Experimental Physics, B. Cheremushkinskaya 25, RU-117259 Moscow, Russia*

We present a unified description of the vector meson and dilepton production in elementary and in heavy ion reactions. The production of vector mesons (ρ, ω) is described via the excitation of nuclear resonances R. The theoretical framework is an extended vector meson dominance model (eVMD). The treatment of the resonance decays $R \mapsto NV$ with arbitrary spin is covariant and kinematically complete. The eVMD thereby includes excited vector meson states in the transition form factors. This ensures correct asymptotics and provides a unified description of photonic and mesonic decays. The resonance model is successfully applied to the ω production in p-p reactions. The same model is applied to the dilepton production in elementary reactions (p-p, p-d). Corresponding data are well reproduced. However, when the model is applied to heavy ion reactions in the BEVALAC/SIS energy range, the experimental dilepton spectra measured by the DLS Collaboration are significantly underestimated at small invariant masses. As a possible solution of this problem, the destruction of quantum interference in a dense medium is discussed. A decoherent emission through vector meson decays enhances the corresponding dilepton yield in heavy ion reactions. In the vicinity of the ρ/ω peak, the reproduction of the data requires further a substantial collisional broadening of the ρ and, in particular, of the ω meson.

I. INTRODUCTION

One of the important questions which theorists face at present is the dependence of hadron properties on medium effects. Medium effects manifest themselves in the modification of widths and masses of resonances produced in nuclear collisions. The magnitude of such changes thereby depends on the density and the temperature of the medium. For example, the proposed Brown-Rho scaling [1] is equivalent to a reduction of the vector meson masses in the nuclear medium. The same conclusion is obtained from QCD sum rules [2] and within effective hadronic models [3]. The dispersion analysis of forward scattering amplitudes [4–7] showed that vector meson mass shifts are in general small and positive, whereas at low momenta they can change the sign, which is in qualitative agreement with the Brown-Rho scaling and the results from QCD sum rules. However, the question of in-medium masses must be finally settled experimentally.

Dilepton spectra from heavy-ion collisions are considered as a suitable tool for this purpose. The CERES [8] and the HELIOS [9] Collaborations measured dilepton spectra at the CERN and found a significant enhancement of the low-energy dilepton yield below the ρ and ω peaks [8] in heavy reaction systems (Pb+Au) compared to light systems (S+W) and proton induced reactions (p+Be). Theoretically, this enhancement can be explained within a hadronic picture by the assumption of a dropping ρ mass [10] or by the inclusion of in-medium spectral functions for the vector mesons [11,12]. In both cases the enhanced low-energetic dilepton yield is not simply caused by a shift of the ρ and ω peaks in the nuclear medium, but it originates to most extent from an enhanced contribution of the $\pi^+\pi^-$ annihilation channel which, assuming vector dominance, runs over an intermediate ρ meson. An alternative scenario could be the formation of a quark-gluon plasma which leads to additional (pQCD) contributions to the dilepton spectrum [11,13].

A similar situation occurs at a completely different energy scale, namely, around 1A GeV incident energies where the low mass region of dilepton spectra are underestimated by the present transport calculations compared to pp and pd reactions. The corresponding data were obtained by the DLS Collaboration at the BEVALAC [14]. However, in contrast to ultrarelativistic reactions (SPS), the situation does not improve when full spectral functions and/or a dropping mass of the vector mesons are taken into account [15,16,12]. This fact is known as the DLS puzzle. The reason lies in the fact that both possible pQCD contributions as well as a sufficient amount of $\pi^+\pi^-$ annihilation processes are absent at intermediate energies. Also a dropping η mass can be excluded as a possible explanation of the DLS puzzle since it would contradict m_T scaling [12]. Furthermore, chiral perturbation theory predicts only very small modifications of the in-medium η mass [17]. Thus one has to search for other sources which could explain the low mass dilepton excess seen in heavy ion reactions. Dilepton spectra were also measured at the KEK in $p+A$ reactions at a beam energy of 12 GeV [18]. Also, here an excess of dileptons compared to the known sources was observed below the ρ-meson peak and interpreted as a change of the vector meson spectral functions. These data were recently analyzed in Ref. [19], again without success to explain the experimental spectrum within a dropping mass scenario and/or by a significant collision broadening of the vector mesons. Since the vector meson peaks are not resolved experimentally [14], the problem to extract in-medium masses directly from experimental data remains extremely difficult.

For all these studies a precise and a rather complete knowledge of the relative weights for the existing decay channels is indispensable in order to draw reliable conclu-

68 014904-1

sions from dilepton spectra. In Ref. [20] a systematic study of meson decay channels was performed, including channels that have been neglected so far, such as, e.g., four-body decays $\rho^0 \to \pi^0 \pi^0 e^+ e^-$. However, as has been shown in Ref. [21] in pp reactions, the contributions of these more exotic channels are not large enough to enhance the low mass dilepton yield at incident energies around $1A$ GeV. Here the low mass dilepton spectrum is dominated by the η and the contributions from the decay of baryonic resonances [15,21,23].

The importance of the resonance contribution to the dilepton yield in elementary and heavy ion reactions has been stressed in several works [21,22,24–33]. In Ref. [33] we calculated in a fully relativistic treatment the dilepton decays $R \to N e^+ e^-$ of nucleon resonances with masses below 2 GeV. Kinematically, complete phenomenological expressions for the dilepton decays of resonances with arbitrary spin and parity, parametrized in terms of the magnetic, electric, and Coulomb transition form factors and numerical estimates for the dilepton spectra and branching ratios of the nucleon resonances were given. In Ref. [21] this approach was applied to the dilepton production in pp reactions at BEVALAC energies. In Sec. II the theoretical framework for the description of the dilepton sources is briefly reviewed. The relevant elementary hadronic reactions are systematically discussed. It is demonstrated that the resonance model provides an accurate description of exclusive vector meson production in nucleon-nucleon collisions $NN \to NN\rho(\omega)$ as well as in pion scattering $\pi N \to N\rho(\omega)$. The resonance model allows further to determine the isotopic channels of the $NN \to NN\rho(\omega)$ cross section where no data are available. We give isospin relations and simple parametrizations of the exclusive $NN \to NN\rho(\omega)$ cross section. As discussed in Ref. [34], a peculiar role thereby plays the $N^*(1535)$ resonance which, fitting available photoproduction data, has a strong coupling to the $N\omega$ channel. Close to threshold this can lead to strong off-shell contributions to the ω production cross section [34], which are also reflected in the dilepton yields. For completeness the dilepton spectra in elementary p-p and p-d reactions are reviewed.

The reaction dynamics of heavy-ion collisions is described within the QMD transport model [35,36] which has been extended, i.e., the complete set of baryonic resonances (Δ and N^*) with masses below 2 GeV has been included in the Tübingen transport code. A short description of the QMD model is given in Sec. IV. One purpose of the present investigations is to extract information on the in-medium ρ- and ω-meson widths directly from the BEVALAC data [14]. The dilepton spectra, distinct from the vector meson masses, are very sensitive to the vector meson in-medium widths, especially the ω meson. The collision broadening is a universal mechanism to increase particle widths in the medium. For example, data on the total photoabsorption cross section on heavy nuclei [37] provide evidence for a broadening of nucleon resonances in a nuclear medium [38]. The same effect should be reflected in a broadening of the vector mesons in dense matter. Since the DLS data show no peak structures which can be attributed to the vector meson masses, the problem to extract information on possible mass shifts is not yet settled. However, the data allow us to estimate the order

of magnitude of the collision broadening of the vector mesons in heavy-ion collisions.

Another question which is addressed in Sec. III is the role of quantum interference effects. Semiclassical transport models such as QMD do not keep track of relative phases between amplitudes but generally assume that decoherent probabilities can be propagated. On the other hand, it has been stressed in several works [27,30] that, e.g., the interference of the isovector-isoscalar channels, i.e., the so-called ρ-ω mixing can significantly alter the corresponding dilepton spectra. The ρ-ω mixing was mainly discussed for the dilepton production in πN reactions. Due to the inclusion of excited mesonic states in the resonance decays, such an interference occurs in our treatment already separately inside each isotopic channel. It is natural to assume that the interference pattern of the mesonic states will be influenced by the presence of surrounding particles. In Sec. III, we discuss qualitatively decoherence effects which can arise when vector mesons propagate through a hot and dense medium. We propose a simple scheme to model this type of decoherence phenomenon where the environment is treated as a heat bath. This discussion is quite general and can be applied, e.g., to the ρ-ω mixing as a special case. It is assumed that before the first collision with a nucleon or a pion, the vector mesons radiate $e^+ e^-$ pairs coherently and decoherently afterwards, since the interactions with a heat bath result in macroscopically different final states. As a consequence of charge conservation the coherence must be restored in the soft-dilepton limit. The present model fulfills this boundary condition. The quark counting rules require a destructive interference between the vector mesons entering into the electromagnetic transition form factors of the nucleon resonances. Hence, a breakup of the coherence results in an increase of the dilepton yield below the ρ-meson peak. This is just the effect observed in the BEVALAC data. That such a quantum decoherence can at least partially resolve the DLS puzzle in heavy-ion reactions is demonstrated in Sec. V.

II. ELEMENTARY SOURCES FOR DILEPTON PRODUCTION

A. Mesonic decays

At incident energies around 1 GeV meson production (except the pion) is a subthreshold process in the sense that the incident energies lie below the corresponding vacuum thresholds. The cross sections for meson production $\mathcal{M} = \eta, \eta', \rho, \omega, \phi$ are small and these mesons (distinct from the pions) do not play an essential role for the dynamics of the heavy-ion collisions. The production of the mesons $\mathcal{M} = \eta, \eta', \rho, \omega, \phi$ can therefore be treated perturbatively. The decays to dilepton pairs take place through the emission of a virtual photon. The differential branching ratios for the decay to a final state $X e^+ e^-$,

$$dB(\mu, M)^{\mathcal{M} \to e^+ eX} = \frac{d\Gamma(\mu, M)^{\mathcal{M} \to e^+ e^- X}}{\Gamma_{tot}^{\mathcal{M}}(\mu)}, \quad (1)$$

where μ is the meson mass and M the dilepton mass are taken from Ref. [20]. These are direct decays $\mathcal{M} \to e^+ e^-$,

Dalitz decays $\mathcal{M} \rightarrow \gamma e^+ e^-$, $\mathcal{M} \rightarrow \pi(\eta) e^+ e^-$, and four-body decays $\mathcal{M} \rightarrow \pi \pi e^+ e^-$. The experimentally known branching ratios are fitted by the vector meson dominance (VMD) model and its extension (see below) used in Ref. [20]. More exotic decay modes such as, e.g., $\phi \rightarrow \pi^0 e^+ e^-$, $\eta \rightarrow \pi^+ \pi^- e^+ e^-$ have recently been measured [39] and are in good agreement with the predictions made in Ref. [20]. The decay modes determined in Ref. [20] including channels which contribute to the background of the dilepton spectra are taken into account.

B. Resonance decays

Usually, the description of the decays of baryonic resonances $R \rightarrow N e^+ e^-$ is based on the VMD model in its monopole form, i.e., with only one virtual vector meson ($V = \rho, \omega$). As a result, the model provides a consistent description of both, radiative $R \rightarrow N \gamma$ and mesonic $R \rightarrow NV$, decays. However, a normalization to the radiative branchings strongly underestimates the mesonic ones [21,25,24]. Possible ways to circumvent this inconsistency were proposed in Ref. [24,25]. In Ref. [24], a version of the VMD model with vanishing $\rho \gamma$ coupling in the limit of real photons ($M^2 = 0$) was used, which allows to fit radiative and mesonic decays independently; in Ref. [25] an additional direct coupling of the resonances to photons was introduced.

However, apart from that, the standard VMD predicts a $1/t$ asymptotic behavior for the transition form factors. At the same time the quark counting rules require a stronger suppression at high t. A similar problem arises with the ω Dalitz decay. The $\omega \pi \gamma$ transition form factor shows an asymptotic $\sim 1/t^2$ behavior [40]. It has been measured in the timelike region [41] and the data show deviations from the naive one-pole approximation. In Ref. [20] it was shown that the inclusion of higher vector meson resonances in the VMD can resolve this problem and provide the correct asymptotics. In Ref. [33] the extended VMD (eVMD) model was used to describe the decay of baryonic resonances and in particular to solve the inconsistency between RNV and $RN\gamma$ decay rates. In the eVMD model one assumes that radial excitations $\rho(1250)$, $\rho(1450)$, ... can interfere with the ground state ρ meson in radiative processes. Already in the case of the nucleon form factors the standard VMD is not sufficient, and radially excited vector mesons ρ', ρ'', ..., etc., should be added in order to provide a dipole behavior of the Sachs form factors and to describe the experimental data [42,43]. In view of these facts, the present extension of the VMD model is more general than the approach pursued in Refs. [24] since it allows not only to describe consistently resonance decays but also other observables such as the ω Dalitz decay or the nucleon form factor. Here we only briefly sketch the basic ideas of the extended vector meson dominance (eVMD) model. In Fig. 1 the resonance decays are schematically displayed for the extended VMD model with excited mesons as intermediate states. The interference between the different meson families plays a crucial role for the behavior of the form factors. Section III will be devoted to this question. Details of the relativistic calculation of the magnetic, electric, and Coulomb transition form factors and the branching
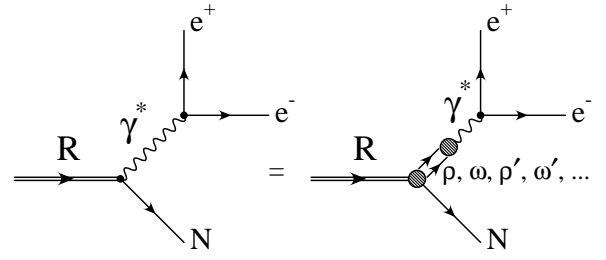

FIG. 1. Decay of nuclear resonances to dileptons in the extended VMD model. The $RN\gamma$ transition form factors contain contributions from ground state and excited ρ and ω mesons.

ratios of the nucleon resonances can be found in Ref. [33]. In terms of the branching ratios for the Dalitz decays of the baryon resonances, the cross section for $e^+ e^-$ production from the initial state X' together with the final state NX can be written as

$$\frac{d\sigma(s,M)^{X' \rightarrow NX e^+ e^-}}{dM^2} = \sum_R \int_{(m_N+M)^2}^{(\sqrt{s}-m_X)^2} d\mu^2 \frac{d\sigma(s,\mu)^{X' \rightarrow RX}}{d\mu^2}$$
$$\times \sum_V \frac{dB(\mu,M)^{R \rightarrow VN \rightarrow N e^+ e^-}}{dM^2}. \quad (2)$$

Here, μ is the running mass of the baryon resonance R with the cross section $d\sigma(s,\mu)^{X' \rightarrow XR}$, $dB(\mu,M)^{R \rightarrow VN \rightarrow N e^+ e^-}$ is the differential branching ratio for the Dalitz decay $R \rightarrow N e^+ e^-$ through the vector meson V. Thus Eq. (2) describes baryon induced and pion induced dilepton production, i.e., the initial state can be given by two baryons ($X' = NN$, NR, $R'R$) or it runs through pion absorption ($X' = \pi N$). In the resonance model both processes are treated on the same footing by the decay of intermediate resonances.

If the width $\Gamma(R \rightarrow N\gamma^*)$ is known, the factorization prescription [20] can be used to find the dilepton decay rate,

$$d\Gamma(R \rightarrow N e^+ e^-) = \Gamma(R \rightarrow N\gamma^*) M \Gamma(\gamma^* \rightarrow e^+ e^-) \frac{dM^2}{\pi M^4}, \quad (3)$$

where

$$M\Gamma(\gamma^* \rightarrow e^+ e^-) = \frac{\alpha}{3}(M^2 + 2m_e^2)\sqrt{1 - \frac{4m_e^2}{M^2}} \quad (4)$$

is the decay width of a virtual photon γ^* into the dilepton pair with the invariant mass M.

In the relativistic version of the eVMD model [33], which is used here as well as in Refs. [21,34], the decay width $\Gamma(R \rightarrow N\gamma^*)$ is described by three independent transition form factors for resonances with spin $J > 1/2$ and by only two transition form factors for spin-1/2 resonances which follows from the number of independent helicity amplitudes. In terms of the electric (E), magnetic (M), and Coulomb (C)

form factors, the decay widths of nucleon resonances with spin $J = l + 1/2$ into a virtual photon with mass M has the form [33]

$$\Gamma(N_{(\pm)}^* \to N\gamma^*) = \frac{9\alpha}{16} \frac{(l!)^2}{2^l(2l+1)!}$$

$$\times \frac{m_\pm^2(m_\mp^2 - M^2)^{l+1/2}(m_\pm^2 - M^2)^{l-1/2}}{\mu^{2l+1} m_N^2}$$

$$\times \left(\frac{l+1}{l} |G_{M/E}^{(\pm)}|^2 + (l+1)(l+2)|G_{E/M}^{(\pm)}|^2 \right.$$

$$\left. + \frac{M^2}{\mu^2} |G_C^{(\pm)}|^2 \right), \tag{5}$$

where μ refers to the nucleon resonance mass, m_N is the nucleon mass, and $m_\pm = \mu \pm m_N$. The signs $\pm$ refer to the natural parity $(1/2^-, 3/2^+, 5/2^-, \dots)$ and abnormal parity $(1/2^+, 3/2^-, 5/2^+, \dots)$ resonances. $G_{M/E}^\pm$ means G_M^+ or G_E^-. The above equation is valid for $l > 0$. For $l = 0$ ($J = 1/2$), one gets

$$\Gamma(N_{(\pm)}^* \to N\gamma^*) = \frac{\alpha}{8\mu}(m_\pm^2 - M^2)^{3/2}(m_\mp^2 - M^2)^{1/2}$$

$$\times \left(2|G_{E/M}^{(\pm)}|^2 + \frac{M^2}{\mu^2}|G_C^{(\pm)}|^2 \right). \tag{6}$$

In Ref. [33] the extended VMD model was applied in a fully covariant form to the description of the transition form factors of the nucleon resonances with arbitrary spin and parity. The decay widths are then given in terms of covariant amplitudes which can be converted to magnetic, electric, and Coulomb transition form factors. To constrain the asymptotics, quark counting rules were used. The free parameters of the model are fixed by fitting the experimental data on the photoproduction and electroproduction amplitudes and by fitting the results of multichannel πN-scattering partial-wave analysis and quark model predictions for these amplitudes. In the relativistic treatment the number of intermediate ρ (or ω) states, which has to be taken into account to describe the magnetic, electric, and Coulomb transition form factors, depends on the resonance spin J; i.e., $J - (1/2) + 3$ mesons have to be included in the minimal version of the eVMD model. Since we consider resonances with spins ranging from 1/2 up to 7/2, the number of ρ states is maximally 6. The following masses have been used: 0.769, 1.250, 1.450, 1.720, 2.150, and 2.350 (in GeV). Within this description dilepton branching ratios were determined quantitatively for baryonic resonances with masses below 2 GeV. In particular, a simultaneous description of radiative and mesonic decays could be achieved. For further details, we refer the reader to Ref. [33].

C. Vector meson production in NN collisions

Cross sections for the direct vector meson production ($V = \rho, \omega, \phi$) in nucleon-nucleon collisions $\sigma^{NN \to XV}$ can, e.g.,

be taken from Refs. [44,45]. These are parametrizations of the inclusive production cross sections in proton-proton reactions ($pp \to XV$) fitted to experimental data in combination with LUND string model predictions [45] and exclusive cross sections determined in a one-pion-exchange picture [44]. However, in heavy-ion reactions at subthreshold energies, i.e., in the BEVALAC and SIS domain, one can expect that significant strength of the dilepton yield originates from the decay of vector mesons (in particular, the ρ) which are far off-shell with masses well below their pole values. Such processes give contributions to the cross sections below the sharp threshold $\sqrt{s_0} = 2m_N + m_V$ with m_V being the pole mass. Subthreshold meson production can be naturally described through the decay of baryonic resonances [21,25–29]. Around threshold the final states consist only of two nucleons and the corresponding meson. These are the processes which are relevant in heavy-ion reactions at intermediate energies in the BEVALAC and GSI range, i.e., at bombarding energies below $2A$ GeV. Due to the moderate incident energies involved in the elementary reactions, it is sufficient to consider exclusive meson production. Since the production of vector mesons through the decay of baryonic resonances gives a significant contribution to the total cross section, thereby one has to avoid the problem of double counting between the dilepton production via baryonic resonances and those originating from other sources. A detailed discussion of the double-counting problem in nucleon-nucleon collisions can be found in Ref. [21].

The vector meson production cross section is now given as follows:

$$\frac{d\sigma(s,M)^{NN \to NNV}}{dM^2} = \sum_R \int_{(m_N+M)^2}^{(\sqrt{s}-m_N)^2} d\mu^2$$

$$\times \frac{d\sigma(s,\mu)^{NN \to NR}}{d\mu^2} \frac{dB(\mu,M)^{R \to VN}}{dM^2}. \tag{7}$$

The cross sections for the resonance production are given by

$$d\sigma(s,\mu)^{NN \to NR} = \frac{|\mathcal{M}_R|^2 p_f}{16 p_i s \pi} dW_R(\mu), \tag{8}$$

with the final center-of-mass (c.m.) momentum

$$p_f = p^*(\sqrt{s}, \mu, m_N) = \frac{\sqrt{[s - (\mu + m_N)^2][s - (\mu - m_N)^2]}}{2\sqrt{s}} \tag{9}$$

and the initial c.m. momentum p_i. The mass distributions $dW_R(\mu)$ of the resonances are the usual Breit-Wigner distributions

$$dW_R(\mu) = \frac{1}{\pi} \frac{\mu \Gamma^R(\mu) d\mu^2}{(\mu^2 - m_R^2)^2 + [\mu \Gamma_{tot}^R(\mu)]^2}, \tag{10}$$

where μ and m_R are the running and pole masses, respectively, and $\Gamma(\mu)$ is the mass dependent resonance width. The
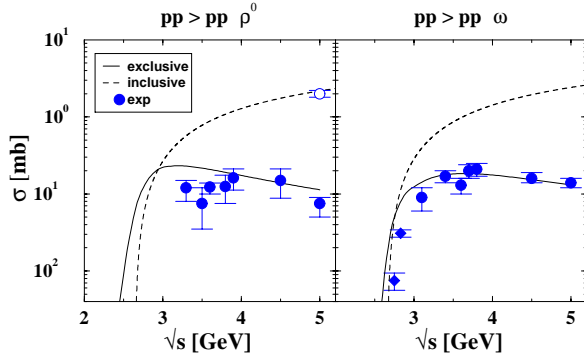
FIG. 2. Cross sections for the ρ^0 and ω production in proton-proton reactions. The exclusive vector meson cross sections through the decay of baryonic resonances are compared to the data and to the inclusive cross sections of Ref. [45]. For ρ^0, also one data point (open circle) for the inclusive cross section is shown. The ω data are taken from Ref. [50] (diamonds) and Refs. [51,52] (circles).

FIG. 3. Differential cross sections $d\sigma/dM$ for the ρ^0 and ω production in proton-proton reactions as a function of the meson mass M. The cross sections are shown for various values of the excess energy $\epsilon = \sqrt{s} - (2m_N + m_V)$, where m_V is given by the ρ and ω pole masses.

matrix elements $\mathcal{M}_R$ are taken from Refs. [46,47], where they have been adjusted to one- and two-pion production data. For the description of the ρ and ω production in NN and πN reactions, we consider the same set of resonances which has been used in Refs. [21,34]. It includes only the well-established (4*) resonances listed by the Particle Data Group (PDG) [48], and is smaller than the complete set of resonances included in the QMD model. This set of resonances is, however, sufficient to describe the NN and πN vector meson production data. The corresponding decay widths $\Gamma_{N\rho}$, $\Gamma_{N\omega}$ at the resonance pole masses are given in Tables III and IV. Off-shell the normalization of the total widths is ensured by the same procedure as used in Ref. [34].

In Fig. 2 the resonance contributions $pp \to pR \to pp\rho^0(\omega)$ to the exclusive ρ^0 and ω production are compared to the inclusive cross section from Ref. [45] and to the corresponding experimental data for the exclusive cross sections. It can be seen from there that the exclusive $pp \to pp\rho^0(\omega)$ cross sections can be saturated by the excitation of intermediate resonances. In the present calculations the dilepton production via the decay of baryonic resonances (2) runs over intermediate vector mesons with mass M, which can be off shell. Therefore, in Eq. (7) the thresholds for the production of a vector meson with mass M are given by the two-pion threshold $2M_N + 2m_\pi$ for ρ, and the three-pion threshold $2M_N + 3m_\pi$ for ω, respectively. This is in contrast to parametrizations of the elementary cross sections [44,45] where vector mesons are produced with sharp thresholds given by their pole masses ($\sqrt{s_0} = 2M_N + m_V$).

The subthreshold production of vector mesons results in a significant strength near $\sqrt{s_0}$ and below. Due to the broad ρ width, this gives the dominant contribution to the total cross section around threshold and explains the differences between our calculation and the parametrization of Ref. [45]. The subthreshold production is of course smaller for ω. However, as discussed, e.g., in Ref. [49] at threshold, also in the case of ω a large amount of the cross section can originate from subthreshold ω production. On the other hand, the inclusion of subthreshold meson production makes the com-
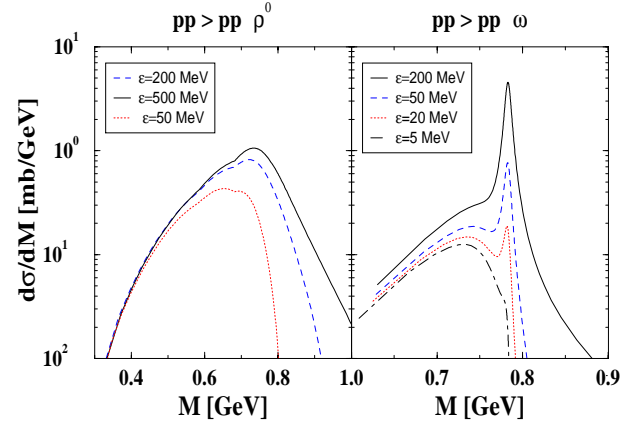
parison with data more difficult since the experimental identification by correlated pions misses strength from such sub-threshold processes [49]. Consequently, two recent data points from the COSY-TOF Collaboration [50] for $pp \to pp\omega$ are overestimated in Fig. 2. However, in pp reactions at low incident energies the subthreshold contribution dominates the dilepton yield in the mass region between the η and the ρ-ω peak [21].

The importance of the subthreshold contributions where the ρ and ω are produced with masses far below their pole values can be estimated from Fig. 3. Here differential cross sections $d\sigma/dM$ are shown as functions of the meson mass M for the same reactions as in Fig. 2. The cross sections are calculated at different energies, and translated into the excess energy $\epsilon = \sqrt{s} - \sqrt{s_0}$. It is clear that close to "threshold" the cross sections are dominated by "subthreshold" production where the vector mesons are produced off shell. The physical thresholds are given by $2m_\pi$ for ρ and $3m_\pi$ for ω, respectively. Experimentally, these off-shell contributions can hardly be distinguished from the general pionic background in coincidence measurements and are generally treated as background. Due to the large ρ width it is nearly impossible to distinguish the ρ peak from this background contribution, which makes it impossible to identify ρ experimentally at small excess energies.

The situation is more complicated for ω. A detailed investigation of the ω production in pp reactions within the framework of the resonance model was performed in Ref. [34]. Among the considered resonances, the $N^*(1535)$ turned out to play a special role for the ω production. The reason is a large decay mode of this resonance to the $N\omega$ channel in a kinematical regime where the ω is far off shell. A strong $N^*(1535)N\omega$ coupling is implied by the available electroproduction and photoproduction data [33]. As a consequence, large off-shell contributions in the ω production cross section appear. In particular, close to threshold, the off-shell production is dominant [34]. This part of the cross section cannot, however, experimentally be identified, and is
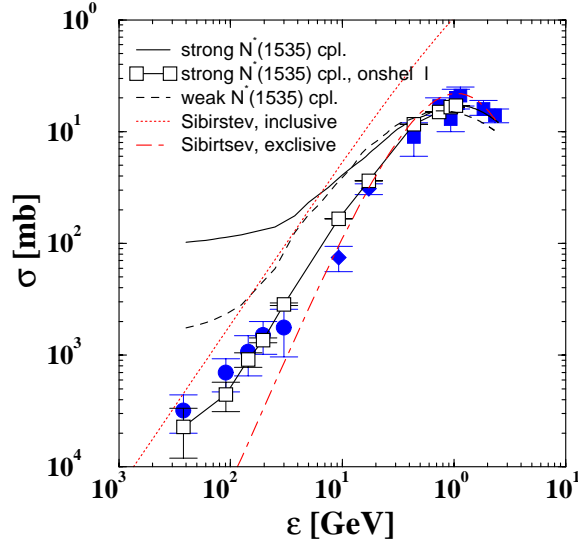
FIG. 4. Exclusive $pp \to pp\omega$ cross section obtained in the resonance model as a function of the excess energy ϵ. The solid curve shows the full cross section [strong $N^*(1535)N\omega$ coupling] including off-shell contributions, while the squares show the experimentally detectable on-shell part of the cross section. The dashed curves show the corresponding cross section obtained with weak $N^*(1535)N\omega$ coupling. The dotted curve is a parametrization of the inclusive cross section from Ref. [45]. Data are taken from Refs. [49,50] and Refs. [51,52].

currently attributed to the experimental background. To compare to the data we applied in Ref. [34] the same procedure as experimentalists: The theoretical "background" from the off-shell production was subtracted and only the measurable pole part of the cross section was taken into account. Doing so, without adjusting any new parameters, the available data are accurately reproduced from energies very close to threshold [49,50] up to energies significantly above the threshold [51,52]. At small excess energies the full cross section shown in Fig. 4 is about one order of magnitude larger than the measurable pole part.

Since the ω cross section depends crucially on the role of the $N^*(1535)$ in Ref. [34], we also considered an alternative possible scenario: The $N\omega$ decay of the $N^*(1535)$ resonance has not directly been measured, and the existing $N\rho$ data leave some freedom to fix the eVMD model parameters. A different normalization to the $N\rho$ channel, thereby making use of an alternative set of quark model predictions, allows to reduce the $N\omega$ decay mode by maximally a factor of $6-8$, however, at the expense of a slightly worse reproduction of the existing dataset. With the reduced $N\omega$ coupling the off-shell contributions are substantially reduced. However, the pole part of the cross section leads to a significant overestimation of the experimental data around and several 100 MeV above the threshold. The ρ production turned out to be practically independent of the choice of the two different parameter sets.

In Ref. [34] we concluded that based on the $pp\omega$ data it would not be possible to decide whether the ω production is accompanied by strong off-shell contributions close to threshold or not, because this part of the cross section is

TABLE I. Coefficients for the isotopic decomposition of the $NN \to NN\rho$ cross section into contributions from Δ and N^* resonances.

	α	β
$pp \to pp\rho^0$	1/6	1/3
$pp \to pn\rho^+$	5/6	2/3
$nn \to nn\rho^0$	1/6	1/3
$nn \to np\rho^-$	5/6	2/3
$np \to np\rho^0$	1/3	1/3
$np \to pp\rho^-$	1/12	1/3
$np \to nn\rho^+$	1/12	1/3

experimentally not accessible. However, these off-shell contributions fully contribute to the dilepton yield from ω decays. Therefore, in Sec. V we consider two different scenarios for the dilepton production through ω decays:

(1) ω production through baryonic resonances with strong $N^*(1535)\omega$ coupling, leading to large off-shell contributions around threshold,

(2) ω production through baryonic resonances with weak $N^*(1535)\omega$ coupling, leading to small off-shell contributions around threshold.

Figure 4 summarizes the different possibilities to treat the ω production in elementary NN reactions. The different cross sections are shown as functions of the excess energy ϵ. The resonance model, assuming a large $N^*(1535)N\omega$ coupling, leads to a very accurate description of the measured on-shell cross section. It has, however, a very strong off-shell component, which fully contributes to the dilepton production. The weak coupling scenario, on the other side, has only small off-shell component, but the reproduction of the data is relatively poor in the low-energy regime. The parametrization of the inclusive cross section $\sigma^{pp \to \omega X} = 2.5(s/s_0 - 1)^{1.47}(s/s_0)^{-1.11}$ [45], which has been used in Refs. [12,23], is also shown for comparison.

If cross sections are based on fits to data isospin factors are usually obtained from the corresponding Clebsh-Gordon coefficients under the assumption of totally isospin independent matrix elements. Such an assumption is, however, crude. It is not possible to fix the two different isospin amplitudes of the ρNN final state and their relative phases solely from measured cross sections and without further model assumptions. In the resonance model the isospin dependence of the cross sections is well defined by coupling the final states to $N \otimes [N \otimes \rho]$. In the $N\rho$ system the $I = 3/2$ amplitude contains all Δ resonances whereas the $I = 1/2$ contains the contributions form the N^*s. Since the resonance amplitudes are summed incoherently, the cross section can be easily decomposed into the corresponding isospin contributions. The isotopic channels of the $NN \to NN\rho$ cross section are then uniquely fixed by

$$\sigma(NN \to NN\rho) = \alpha\sigma_{3/2} + \beta\sigma_{1/2}, \qquad (11)$$

where α, β are determined from the corresponding Clebsh-Gordon coefficients. The coefficients are summarized in Table I. Figure 5 shows the corresponding contributions $\sigma_{3/2}$
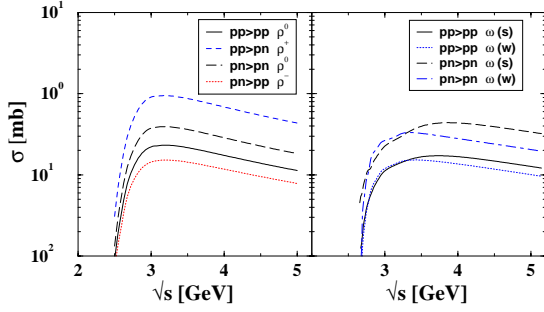
FIG. 5. Left: isospin dependence of the exclusive $NN \rightarrow NN\rho$ cross section assuming isospin independent matrix elements for the resonance production. Right: isospin dependence of the exclusive $NN \rightarrow NN\omega$ cross section. The isospin dependence of the $N^*(1535)$ is taken into account. We distinguish between a strong (s) and a weak (w) $N^*(1535)N\omega$ coupling.

and $\sigma_{1/2}$ originating from the sum over Δ and N^* resonances, respectively, and the different isospin channels of the $NN \rightarrow NN\rho$ cross section. The isospin dependence is significant. The $pn \rightarrow pn\rho^0$ channel is about two times and the $pn \rightarrow pn\rho^+$ about four times larger than the measured $pp \rightarrow pp\rho^0$ channel.

The two isotopic channels $\sigma_{3/2}$ and $\sigma_{1/2}$ can be parametrized in the form

$$\sigma_{3/2,1/2} = \frac{a_1(\sqrt{s} - a_2)^{a_3}}{(\sqrt{s} - a_4)^2 + a_5}, \tag{12}$$

with the coefficients $a_1 = 0.7813$ (0.334), $a_2 = 2.512$ (2.508), $a_3 = 1.206$ (1.135), $a_4 = 2.736$ (2.426), and $a_5 = 0.293$ (0.412) for the $I = 3/2(1/2)$ channels. A parametrization of $\sigma(pp \rightarrow pp\omega)$ by Eq. (12) yields the following coefficient: $a_1 = 0.4921$, $a_2 = 2.656$, $a_3 = 0.7529$, $a_4 = 2.6812$, and $a_5 = 1.8395$. Note that the thresholds for the parametrizations (12) are given by the a_2 values and account only partially for the subthreshold contributions in the cross sections.

The isotopic relations given in Tables I and II are derived under the assumption of isospin independent matrix elements

TABLE II. Coefficients for the isotopic decomposition of the $\pi N \rightarrow \rho N$ cross section into contributions from Δ and N^* resonances.

	α	β
$\pi^+ p \rightarrow \rho^+ p$	1	0
$\pi^+ n \rightarrow \rho^+ n$	1/9	4/9
$\pi^+ n \rightarrow \rho^0 p$	2/9	2/9
$\pi^0 p \rightarrow \rho^+ n$	2/9	2/9
$\pi^0 p \rightarrow \rho^0 p$	4/9	1/9
$\pi^0 n \rightarrow \rho^0 n$	4/9	1/9
$\pi^0 n \rightarrow \rho^- p$	2/9	2/9
$\pi^- p \rightarrow \rho^0 n$	2/9	2/9
$\pi^- p \rightarrow \rho^- p$	1/9	4/9
$\pi^- n \rightarrow \rho^- n$	1	0

$\mathcal{M}_R$ for the resonance production (8). This assumption is justified for all resonances except the $N^*(1535)$ [46]. For this resonance the $pn \rightarrow pn^*(np^*)$ cross section is known to be about five times larger than for $pp \rightarrow pp^*$ [46]. This fact is also reflected in the isotopic relation for the η production to which the $N^*(1535)$ has a large branching ratio. If we take the enhancement of the $N^*(1535)$ matrix element in the pn channel by a factor of 5 into account, the $pn \rightarrow pn\rho^0$ cross section shown in Fig. 5 is shifted upwards by 10% and the $pn \rightarrow pp\rho^-$ cross section by 20%.

For the ω production only N^* resonances contribute, and thus the naive isospin relation would imply $\sigma(pn \rightarrow pn\omega) = \sigma(pp \rightarrow pp\omega)$. However, in this case the strongly isospin dependent $N^*(1535)$ production cross section has a large influence, which depends of course on the strength of the $N^*(1535)N\omega$ coupling. In the case of a weak coupling, the $pn \rightarrow pn\omega$ channel is enhanced by a factor 2, in the case of a strong coupling even by a factor of 3. For all other resonances which contribute to the $NN \rightarrow NN\omega$ cross section shown in Fig. 5 (right), isospin symmetric matrix elements are assumed.

D. Vector meson production in πN collisions

Similar as in the previous case, the pion induced vector meson production can be parametrized and fitted to existing data. For example, in Ref. [45] the exclusive and inclusive $\pi N \rightarrow N\rho(\omega, \phi)$ cross sections have been fitted to data and LUND string model predictions. In the present work we again describe the exclusive cross sections microscopically within the resonance model,

$$\frac{d\sigma(s,M)^{\pi N \rightarrow NV}}{dM^2} = \sum_R d\sigma(s,\mu)^{\pi N \rightarrow R} \frac{dB(\mu,M)^{R \rightarrow VN}}{dM^2}$$

$$= \sum_R \frac{(2j_R + 1)}{(2j_N + 1)} \frac{\pi^2}{p_i^2} \Gamma_{N\pi}^R(\mu) dW_R(\mu)$$

$$\times \frac{dB(\mu,M)^{R \rightarrow VN}}{dM^2}, \tag{13}$$

where j_R is the resonance spin, j_N the nucleon spin, and p_i the πN c.m. momentum. As in the previously discussed NN reactions, the cross sections are calculated as an incoherent sum over all resonances. The same approximation has also been used in other works [25]. Figure 6 shows the corresponding $\pi^+ p \rightarrow p\rho^+$ and $\pi^+ n \rightarrow p\omega$ cross sections. At laboratory momenta below 1.5 GeV, the existing data are generally well reproduced. Close to threshold the same phenomenon as in the NN reactions occurs, i.e., the off-shell meson production gives a large contribution to the total cross section. Again low-energy data which exist in the case of the ω are overpredicted by the calculations. At higher energies the agreement with experiment is very reasonable, both for ρ and ω. However, at momenta above 1.5–2 GeV, the data are generally underpredicted.

As also can be seen form Fig. 11, the total $\pi^+ p \rightarrow X$ and $\pi^- p \rightarrow X$ cross sections can only be well described up to
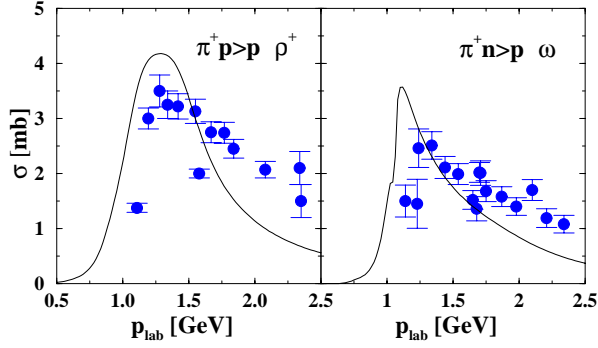
FIG. 6. Exclusive $\pi^+p \to p\rho^+$ and $\pi^+n \to p\omega$ cross sections obtained within the resonance model. The experimental $\pi^+p \to p\rho^+$ are taken from Ref. [53].

pion laboratory momenta around 1.2–1.5 GeV. For the determination of the inclusive pion cross sections, all baryonic resonances given in Tables III, IV are taken into account. Nevertheless, at large p_{lab} the contributions of even higher lying resonances or other direct processes seem to be missing. In the determination of the vector meson production cross sections we rely on the same set of resonances which has been used for NN reactions dicussed in the preceding section. Thus some of the higher lying and insecure resonances included in Fig. 11 are not taken into account here. A substantial missing strength in the $\pi N \to N\omega$ cross section at large values of p_{lab} has also been found in Ref. [25]. Compared to Ref. [25], our results for the cross sections are generally somewhat larger, and thus in better agreement with the data. The reason lies in a different determination of the resonance decay modes to vector mesons within the extended vector dominance model [21].

As in the case for the NN reaction, isospin relations are determined by the composition into contributions from Δ and N^* resonances. Using the same representation as in Eq. (11), $\sigma(\pi N \to N\rho) = \alpha\sigma_{3/2} + \beta\sigma_{1/2}$, the corresponding isospin coefficients are given in Table II.

In summary, at high energies one has to restrict oneself to phenomenological fits to data [45] or include string model

TABLE IV. List of Δ resonances which are included in the QMD transport model. The table shows the resonance masses and the total and partial widths of the included decay channels in MeV. The values of $\Gamma_{N\rho}$ are given at the resonance pole masses. The values in brackets as well as the other decay channels are taken from [47] and used for the reaction dynamics.

Resonance	Mass (MeV)	Γ_{tot} (MeV)	$N\rho$	$N\pi$	$\Delta_{1232}\pi$	$N_{1440}\pi$
Δ_{1232}	1232	115	~ 0	115		
Δ_{1600}	1700	200		30	110	60
Δ_{1620}	1675	180	16.4	45	108	27
Δ_{1700}	1750	300	47.7(30)	60	165	45
Δ_{1900}	1850	240	(36)	72	72	60
Δ_{1905}	1880	363(280)	307.3(168)	56	28	28
Δ_{1910}	1900	250	(100)	87.5	37.5	25
Δ_{1920}	1920	150	(45)	22.5	45	37.5
Δ_{1930}	1930	250	(62.5)	50	62.5	75
Δ_{1950}	1950	250	(37.5)	112.5	50	50

^{a}At the resonance pole, $\Gamma_{N\rho}$ is practically zero for the Δ_{1232} due to vanishing phase space. However, the ρ-meson coupling constants of this resonance, in particular the magnetic one, are large [33], and thus Δ_{1232} has nonvanishing off-shell contributions.

excitations. For the SIS energy domain where vector mesons are predominantly produced, subthreshold the present model gives a reliable description of the vector meson production in πN reactions.

E. Dilepton production in pp and pd reactions

Before turning to heavy-ion collisions, we will consider the dilepton production in elementary reactions. Dilepton spectra in proton-proton and proton-deuteron reactions have been measured by the DLS Collaboration in the energy range $T = 1-5$ GeV [54]. The application of the present model to the dilepton production in pp reactions has in detail been discussed in Ref. [21]. For completeness, we show the corresponding results and the comparison to the DLS data [54]

TABLE III. List of N^* resonances which are included in the QMD transport model. The table shows the resonance masses and the total and partial widths of the included decay channels in MeV. The values of $\Gamma_{N\omega}$ and $\Gamma_{N\rho}$ are given at the resonance pole masses. The values in brackets as well as the other decay channels are taken from Ref. [47] and used for the reaction dynamics.

| Resonance	Mass (MeV)	Γ_{tot} (MeV)	$N\omega$	$N\rho$	$N\pi$	$N\pi\pi$	$\Delta_{1232}\pi$	$N_{1440}\pi$	$N\eta$
N_{1440}	1440	200	$<10^{-4}$	0.45	140	10	50		
N_{1520}	1520	125	0.08	26.63	75	18.75	31.25		
N_{1535}	1535	150	2.05	4.62	82.5	7.5		7.5	52.5
N_{1650}	1650	150	0.94	3.17	97.5	7.5	15	7.5	7.5
N_{1675}	1675	140	0.003	3.50	63	77			
N_{1680}	1680	120	0.50	10.24(24)	78	18			
N_{1700}	1700	100		(5)	10	45	35		5
N_{1710}	1710	110		(5.5)	16.5	22	22	11	22
N_{1720}	1720	184(150)	32.4	129.3(37.5)	22.5	67.5	15		
N_{1900}	1870	500	(275)	(25)	175		25		
N_{1990}	1990	550		(82.5)	27.5	137.5	165	82.5	
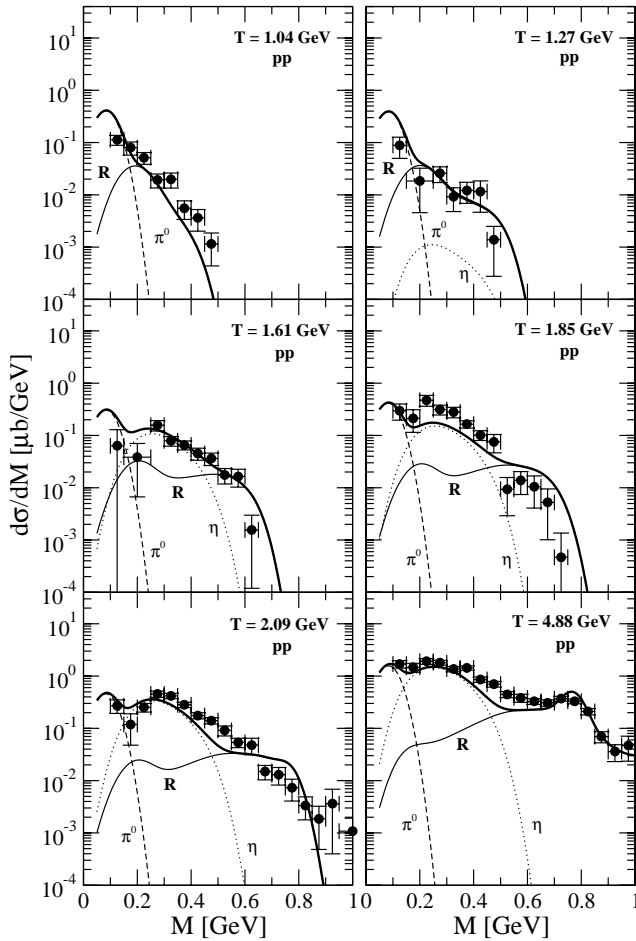
FIG. 7. The differential $pp \rightarrow e^+ e^- X$ cross sections at various proton kinetic energies are compared to the DLS data [54].

in Fig. 7. The agreement with the available data is generally reasonable, i.e., of similar quality as obtained in previous calculations by Ernst *et al.* [15] and Bratkovskaja *et al.* [28]. As in Ref. [15] we observe a slight underestimation of the experimental dilepton yield at the two highest energies $T = 2.09$ and 4.88 GeV in the mass region below the ρ-ω peak. Here the knowledge of the inclusive cross section with multipion final channels starts to play an important role. In Ref. [21] the multipion production was estimated within a semi-empirical model that is slightly modified in the present case. However, results are very similar to our previous calculations [21].

It should be noted that the dilepton yields in pp reactions were obtained with the strong $N^*(1535)$-$N\omega$ decay mode. As briefly described in Sec. II and in detail discussed in Ref. [34], the strong coupling mode is the result of the eVMD fit to the available photoproduction and meson-production data [33]. It leads to sizable contributions from off-shell ω production around threshold energies which are, however, experimentally not accessible in $pp \rightarrow pp\omega$ measurements. On the other side, these off-shell ω's fully contribute to the dilepton yield. The off-shell contributions generally lead to an enhancement of the dilepton yield in the mass region below the ω peak, in particular at incident energies where the ω is dominantly produced subthreshold. In contrast to Refs.

[15,28] where ω is treated as an elementary particle (with fixed mass $m_\omega = 782$ MeV) in our approach the off-shell ω production starts at the three-pion threshold. Thus subthreshold ω production appears already in elementary reactions. As can be seen from Fig. 7 the scenario of large off-shell ω contributions which are the consequence of the strong $N^*(1535)$-$N\omega$ coupling are consistent with the experimental pp dilepton yields in the energy range of $T = 1.04$–1.61 GeV. At higher energies this off-shell production becomes negligible [34].

The situation becomes more complicated when proton-deuteron reactions are considered. Compared to the pp case one has here two important modifications: First, the Fermi motion of the proton and neutron constituents inside the deuteron, and second, the isotopic relations between the pp and pn contributions to the dilepton production. Only few isotopic relations for the meson production are experimentally fixed. Most isospin relations have to be derived from model assumptions (see also Sec. II). For the dilepton production in pN collision we distinguish generally between three different channels,

$$pN \rightarrow NR \rightarrow NN\pi^0; \quad \pi^0 \rightarrow \gamma e^+ e^-,$$

$$pN \rightarrow NR \rightarrow NN\eta; \quad \eta \rightarrow \gamma e^+ e^-,$$

$$pN \rightarrow NR \rightarrow NNe^+ e^-,$$

where R is either a nucleon resonance N^* or a Δ resonance. The last channel contains all contributions which run over intermediate ρ and ω mesons. For the first channel we use here the following isotopic relation for fixed two-nucleon final states (NN); $pp:pn = 1:1(5)$ if the intermediate resonance is $R = N^*[N^*(1535)]$ and $pp:pn = 1:2$ for $R = \Delta$ [46]. To the η production only the $N^*(1535)$ contributes [46], and thus the isotopic relation is $pp:pn = 1:5$. The third channel has the same isotopic relations as the first channel if one assumes that intermediate ρ and ω mesons are not interfering effectively in the pn collision. The latter means that for two equally probable reactions $pn \rightarrow pR^0$ and $pn \rightarrow nR^+$, the radiative decays of R^0 and R^+ resonances have no ρ-ω interference when summed. Then the isospin relations for the ρ^0 and ω can be read from Table I. The Fermi motion of the constituents inside the deuteron is taken into account using the experimental momentum distribution of the bound proton, which was obtained by electron scattering [55].

At the two lowest incident proton energies of $T = 1.04$ GeV and $T = 1.27$ GeV, the threshold effects for the η production become extremely important. For a target nucleon at rest, the η production is far below threshold at $T = 1.04$ GeV ($\epsilon = -84$ MeV, ϵ is the excess energy in the center-of-mass system) and slightly above threshold at $T = 1.27$ GeV ($\epsilon = 6.4$ MeV). The Fermi motion of the proton and neutron constituents inside the deuteron increases the accessible ϵ values. In the present calculations experimental results from electron scattering [55] are used to model the proton and neutron momentum distributions. It is further known from experiment [56] that close to threshold the pn
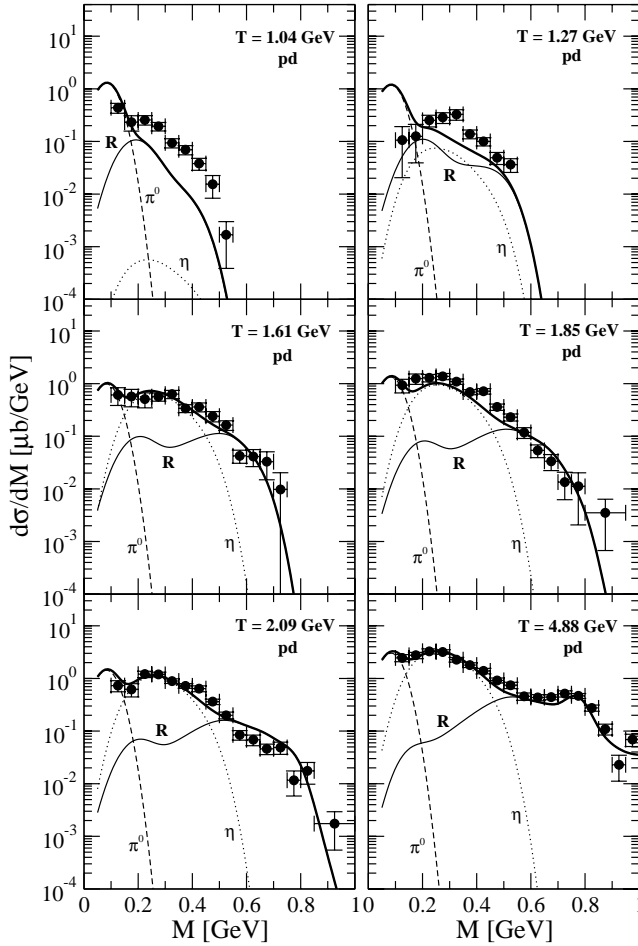
FIG. 8. Experimental data on near to the threshold cross sections of the reactions: $pp \to pp\,\eta$ (circles) [58–62], $pn \to pn\,\eta$ (triangles), and $pn \to d\,\eta$ (squares) were taken from Ref. [56]. The curves show the corresponding model cross sections.

$\to d\eta$ cross section is much larger (by a factor of 3–4) than the $pn \to pn\,\eta$ cross section, which in turn is much larger than the $pp \to pp\,\eta$ cross section (by a factor of 6.5), see Fig. 8. The above channels for the η-meson production take the $pn \to pn\,\eta$ and $pp \to pp\,\eta$ reactions into account [$N^*(1535)$ is produced with appropriate cross sections [46] in pp and pn collisions], but this treatment does not describe properly the reaction $pn \to d\,\eta$, which is dominant near the η threshold. At the two lowest incident proton kinetic energies $T = 1.04$ GeV and $T = 1.27$ GeV, we add therefore the reaction $pn \to d\,\eta$ to the η production sources by a parametrization of the experimental cross section [56]. At higher incident energies ($T = 1.61$–4.88 GeV), the $pn \to d\,\eta$ cross section is not known experimentally, but it is natural to expect that the enhancement of the cross section by the proton-neutron intial/final state interaction (ISI/FSI) in the deuteron becomes negligible at high energies. We therefore omit the reaction $pn \to d\,\eta$ at $T = 1.61$–4.88 GeV.

The results are presented in Fig. 9. At incident kinetic proton energies of $T = 1.04$–2.09 GeV, dileptons are mainly produced from the exclusive reactions mentioned above (exceptions are the π^0 production at $T = 1.85$ GeV, and T
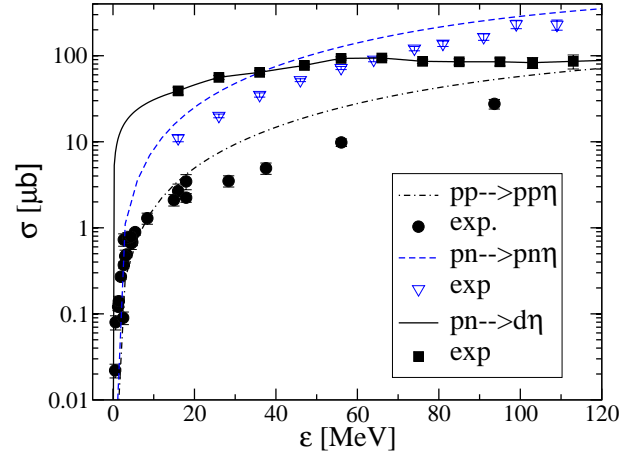

FIG. 9. The differential $pd \to e^+ e^- X$ cross sections at various proton kinetic energies are compared to the DLS data [54].

$= 2.09$ GeV and the η production at $T = 2.09$ GeV). At $T = 4.88$ GeV this procedure strongly underestimates the experimental data. The reason is clear: here the inclusive reactions of $\pi^0, \eta, \rho, \omega$ production become much larger than the exclusive ones. As discussed above, the resonance model provides only exclusive vector meson production cross sections and the corresponding dilepton production cross sections. In the calculations shown in Figs. 7 and 9, we accounted for the inclusive cross sections that play a dominant role at high incident energies in a simple manner: the ratios of the inclusive/exclusive cross sections for $\pi^0-, \eta-, \rho-, \omega$-meson production from the theoretical predictions of Ref. [15] are derived, and our exclusive cross sections are scaled by the corresponding factors. The shape of the experimental curve at $T = 4.88$ is then well reproduced.

At $T = 1.04$ GeV and $T = 1.27$ GeV we strongly underestimate the experimental pd data. This is particularly surprising since the corresponding pp data are reasonably well reproduced. The comparison with other available theoretical calculations [15,28] shows the following: our $\Delta(1232)$ contribution is 2–2.5 times smaller than that of Refs. [15,28]. Comparing the η contributions to the pd dilepton spectrum from Refs. [15]: [28]:[present] yields the following ratios: $40 : 200 : 6$ at $T = 1.04$ GeV and $4 : 15 : 8$ at $T = 1.27$ GeV. However, the large difference of the η meson contributions at $T = 1.04$ GeV does not significantly influence the total dilepton yield since the absolute η contribution is extremely small here. The large difference in the various treatments can be attributed to the high momentum tails of the Fermi motion in the deuteron, which are experimentally not determined, and to different $pp:pn$ ratios. The same is probably true at $T = 1.27$ GeV where the differences concerning the η contributions $(4:15:8)$ are smaller. However, this reflects the amount of uncertainty inherent in the theoretical description of the η production in the pd system around threshold. Nevertheless, the isotopic relations and the treatment of the Fermi motion can be checked calculating the ratio $\sigma(pd \to \eta X)/\sigma(pp \to \eta X)$ at two energies of $T = 1.3$ GeV and $T = 1.5$ GeV, where experimental data on these ratios are available [57]. Our results are

$$\frac{\sigma(pd \to \eta X)}{\sigma(pp \to \eta X)} = (1+5)(2.0), \quad T = 1.3 \text{ GeV},$$

$$\frac{\sigma(pd \to \eta X)}{\sigma(pp \to \eta X)} = (1+5)(0.9), \quad T = 1.5 \text{ GeV},$$

where the first factor originates from the pn isospin relation and the second factor is due to the Fermi motion inside the deuteron. The corresponding experimental values [57] of ≈ 10 and ≈ 5, respectively, demonstrate that the present treatment of the η production is reasonable.

A second deviation between the present approach and the former calculations of Refs. [15,28] is harder to understand. It concerns the contribution of the $\Delta(1232)$ at low energies. In the present treatment the dilepton yield from the $\Delta(1232)$ in pd reactions is by about a factor 2]–2.5 smaller than in Refs. [15,28]. Concerning the $\Delta(1232)$ there exists no sizable influence of the Fermi motion in the deuteron since the reaction is well above the kinematical threshold. A comparison of the $pd:pp$ ratios for the $\Delta(1232)$ yields approximately $(pd:pp)_\Delta \approx 5:1$ in Refs. [15,28], whereas we obtain $(pd:pp)_\Delta \approx 3:1$. This latter result is probably closer to the required isotopic relation. The simplest way to obtain this isotopic relation is the following: the deuteron has a total isospin of $I=0$, and the incoming proton has $I=1/2$. Therefore, the final $NN\Delta$ system should have a total isospin of $I=1/2$. The isotopic wave function of such a system is unique, i.e., it corresponds to Δ^{2+}, Δ^+, and Δ^0 isobars in the proportion $\Delta^{2+}:\Delta^+:\Delta^0 = 3x:2x:1x$. Here x is a factor which accounts effectively for the Fermi motion of the deuteron constituents. It is only written for the comparison to the $pp \to N\Delta$ reaction. Let us compare this result to the Δ contribution in $pp \to N\Delta$ reaction. We now have $\Delta^{2+}:\Delta^+ = 3:1$. Radiative decays occur only for Δ^+ and Δ^0, and the radiative widths are equal. Thus one gets $(pd:pp)_\Delta = 3x:1 \approx 3:1$ due to $x \approx 1$. At $T=1.04$; 1.27 GeV this is an upper limit, i.e., $x<1$, since $NN \to N\Delta$ is almost on top of the cross section.

In summary, the present model reproduces the dilepton production in pd collisions at $T=1.61$–4.88 GeV to be rather reasonable. At the two lowest energies $T=1.04$; 1.27 GeV we underestimate the pd data (probably due to an underestimation of the η contribution). At these energies an underestimation which is, however, less pronounced, was also observed in Ref. [15]. It should be noted that for the pp reactions the present results and those of Ref. [15,28] coincide more or less. In all cases the theoretical calculations reproduce the corresponding DLS data reasonably well. Hence the dilepton production on the deuteron turns out to be rather involved at subthreshold energies due to strong ISI/FSI effects. The pd system is therefore only of limited use to check isospin relations of the applied models. Another important result is the fact that the scenario of large off-shell ω contributions from the $N^*(1535)$-$N\omega$ decay is consistent with the available pp and pd dilepton data.

III. DECOHERENCE AS A MEDIUM EFFECT

In this section we discuss an in-medium modification of the cross section $NN \to e^+e^-X$, which is connected with the decoherence of vector mesons propagating in a hot and dense nuclear medium. In Refs. [21,33], radially excited ρ and ω mesons were introduced in the transition form factors $RN\gamma$ to ensure the correct asymptotic behavior of the amplitudes in line with the quark counting rules. Thereby, we required a destructive interference between the members of the vector meson families away from the poles of the propagators, i.e., the meson masses. In a dense medium the environment of the vector mesons can be regarded as a heat bath. Usually the different scattering channels of the interaction with a heat bath, i.e., the surrounding nucleons and pions, are summed up decoherently since the various channels acquire large uncorrelated relative phases. In such a case, the coherent contributions to the probability are random and cancel each other. We have in a sense macroscopically different intermediate states that do not interfere since small perturbations result in macroscopically large variations of the relative phases. The interaction of the vector mesons with the surrounding particles should therefore breakup the coherence between the corresponding amplitudes for the dilepton production. The break up of the destructive interference results in an increase of the total cross sections at low dilepton masses. In the following, we want to investigate if the decoherence effect can explain the enhancement observed in the dilepton spectra at the BEVALAC experiment (DLS puzzle). Below we put this idea on a more quantitative basis.

A. In-medium modification of the transition form factors

The decay widths of nucleon resonances with spin $J=l+1/2$ and mass μ into a nucleon with mass m_N and a dilepton pair with mass M are described by Eqs. (3)–(6). These widths are proportional to squares of the magnetic (M), electric (E), and Coulomb (C) form factors, $G_T^{(\pm)}(M^2)$ ($T=M,E,C$). In the eVMD model, the transition form factors $RN\gamma$ are written as

$$G_T^{(\pm)}(M^2) = \sum_k \mathcal{M}_{Tk}^{(\pm)}. \tag{14}$$

The sum runs over the ground state and excited ρ and ω mesons. The amplitude

$$\mathcal{M}_{Tk}^{(\pm)} = h_{Tk}^{(\pm)} \frac{m_k^2}{m_k^2 - im_k\Gamma_k - M^2} \tag{15}$$

describes the contribution from the kth vector meson to the type-T decay width. The quark counting rules [40,63] predict the following asymptotics for the covariant form factors of $J \geqslant 3/2$ nucleon resonances:

$$-lG_{E/M}^{(\pm)}(M^2) \simeq G_{M/E}^{(\pm)}(M^2) \sim O\left(\frac{1}{(-M^2)^{l+1}}\right),$$

$$G_C^{(\pm)}(M^2) \sim O\left(\frac{1}{(-M^2)^{l+2}}\right). \qquad (16)$$

These relations provide constraints to the residues $h_{Tk}^{(\pm)}$ and imply a destructive interference between the different members of the vector meson families.

For spin $J = \frac{1}{2}$ resonances one obtains the following asymptotics:

$$G_{E/M}^{(\pm)}(M^2) \sim O\left(\frac{1}{(-M^2)^2}\right), \quad G_C^{(\pm)}(M^2) \sim O\left(\frac{1}{(-M^2)^3}\right). \qquad (17)$$

In the case of a full decoherence the vector meson contributions to the cross section, $NN \to e^+ e^- X$, which run over nucleon resonances, must be summed up decoherently. This leads to the replacement

$$\left| \sum_k \mathcal{M}_{Tk}^{(\pm)} \right|^2 \to \sum_k |\mathcal{M}_{Tk}^{(\pm)}|^2. \qquad (18)$$

As a consequence, total decoherence will result in an enhancement of the resonance contributions due to the presence of the medium. The prescription (18) refers to the limit of full decoherence, i.e., collisions with nearest neighbors occur always before the dilepton emission. However, in reality, both the density and the meson wavelengths are finite; and thus it is necessary to have a relation for the decoherence effect, which is valid in an intermediate regime for densities and the meson wavelengths. The basic assumption is that each of the propagated vector mesons radiates $e^+ e^-$ pairs coherently up to its first collision with a nucleon (or generally a hadron), and incoherently afterwards. This leads to the destruction of the coherence of one meson with the others, which, by themselves, may still form a coherent state. The problem receives at this stage a combinatorial character.

The decay probability for a resonance at distance l_D in the interval dl_D equals

$$dW_D(l_D) = e^{-l_D/L_D} \frac{dl_D}{L_D}. \qquad (19)$$

The decay length for a resonance with lifetime T_D equals $L_D = v \gamma T_D$, where $T_D = 1/\Gamma$, Γ being the total vector meson vacuum width. The collision probability at a distance l_C in the interval dl_C equals

$$dW_C(l_C) = e^{-l_C/L_C} \frac{dl_C}{L_C}. \qquad (20)$$

The collision length L_C is defined by the expression

$$L_C = \frac{1}{\rho_B \sigma}, \qquad (21)$$

where σ is the total VN cross section and ρ_B is the nuclear density.

The meson decay takes place before the first collision, provided that $0 < l_D < l_C$, so the probability of the coherent decay equals

$$w = \int_0^{+\infty} \frac{dl_C}{L_C} e^{-l_C/L_C} \int_0^{l_C} \frac{dl_D}{L_D} e^{-l_D/L_D} = \frac{L_C}{L_C + L_D}. \qquad (22)$$

All mesons have in general different values L_D and L_C, and thus the coherent decay probabilities are different as well. Therefore below the index k is attached to the decay and scattering lengths and to the coherent decay probabilities. In order to account for the decoherence, one should make the replacements

$$|G_T^{(\pm)}(M^2)|^2 \to E_T^{(\pm)}(M^2, \mathbf{Q}^2) |G_T^{(\pm)}(M^2)|^2 \qquad (23)$$

in Eqs. (5) and (6). The enhancement factor $E_T(M^2, \mathbf{Q}^2)$ is given by

$$E_T^{(\pm)}(M^2, \mathbf{Q}^2) = \left(\prod_k w_k \left| \sum_k \mathcal{M}_{Tk}^{(\pm)} \right|^2 + \sum_l (1 - w_l) \right.$$
$$\times \prod_{k \neq l} w_k \left(|\mathcal{M}_{Tl}^{(\pm)}|^2 + \left| \sum_{k \neq l} \mathcal{M}_{Tk}^{(\pm)} \right|^2 \right) + \cdots$$
$$\left. + \prod_l (1 - w_l) \sum_k |\mathcal{M}_{Tk}^{(\pm)}|^2 \right) /$$
$$\left(\left| \sum_k \mathcal{M}_{Tk}^{(\pm)} \right|^2 \right). \qquad (24)$$

It depends on square of the spacelike part $\mathbf{Q}$ of the vector meson momentum through Eq. (21). The first term in Eq. (24) in the numerator corresponds to the probability that all ρ-mesons radiate the dilepton pairs coherently. The second term corresponds to the probability that the lth meson decays to the dilepton pair after its first collision, while the other mesons radiate before the first collision. Finally, the last term corresponds to the probability for an incoherent radiation of all vector mesons. Each term in Eq. (24) contains the squares of the amplitudes $\mathcal{M}_{Tk}^{(\pm)}$ according to the proper interference pattern. If the probability for the coherent radiation equals $w_k = 1$, i.e., the collision length L_C is infinite like in the vacuum, then the vacuum result is recovered, $E_T^{(\pm)}(M^2, \mathbf{Q}^2) = 1$. If the collision length goes to zero, the $w_k = 0$ (full decoherence), and prescription (18) is valid. In the case of isospin $I = 1/2$ resonance decays, Eq. (21) also takes the decoherence between ρ and ω mesons into account.

In order to illustrate the effect of the enhancement factor, we consider the Coulomb form factor for a spin-1/2 Δ resonance where the formulas are simplest. According to the minimal eVMD, three ρ mesons are needed to ensure the correct asymptotics of the transition form factors, i.e., the ground state and the excited $\rho(1250)$ and $\rho(1450)$. Let us take $L_D \approx T_D = 1/\Gamma$, $w_1 = w_2 = w_3$, and vary the collision length L_C from 0 (total decoherence) to ∞ (total coherence). The decoherence factor is plotted in Fig. 10 as a function of the running mass M in the no-width approximation for the ρ mesons. As can be seen from Fig. 10, the decoherence will
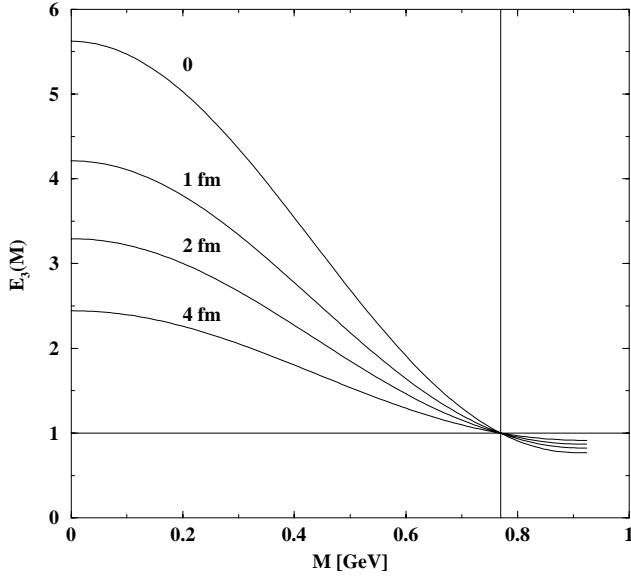
FIG. 10. The enhancement factor $E_C(M)$ for the spin-1/2 $\Delta \rightarrow N e^+ e^-$ Coulomb transition due to the decoherence between the ρ mesons in the medium, estimated within the eVMD model for different values of the mean free path L_C of the ρ mesons in the medium. Three ρ mesons interfere.

generally lead to an enhancement of the dilepton yield in the low-mass region below the ρ peak. It should be noted that a similar effect exists for the dilepton decays of the mesons. Such decays have also constraints from the quark counting rules on the asymptotic behavior of the transition form factors. The decay modes $P \rightarrow e^+ e^- \gamma$, where $P = \pi$, η and $\rho^0 \rightarrow e^+ e^- \pi^+ \pi^-$ have monopole form factors in the amplitudes. To obtain a monopole form factor, it is sufficient to consider only a single ρ meson. In this case no enhancement occurs, i.e., $E(M^2, \mathbf{Q}^2) \equiv 1$. The decay modes $V \rightarrow e^+ e^- P$, $\eta \rightarrow e^+ e^- \pi^+ \pi^-$, and $\rho^0(\omega) \rightarrow e^+ e^- \pi^0 \pi^0$, with dipole form factors, require the existence of at least two ρ states. In such a minimal case, these modes are enhanced. However, the decays of the last type are nondominant, and their enhancement is not taken into account in the simulations.

B. Restoration of coherence in the soft-dilepton limit

Physically, if many nucleons appear on the scale of the mesonic wavelength, the scattering process must have a coherent character with respect to clusters formed by the surrounding nucleons. In such a case, Eq. (21) does not apply any more. The eVMD model can also be used for the description of the diagonal electromagnetic form factors. When $M = \mathbf{Q}^2 = 0$, the diagonal form factors, e.g., of the nucleon, measure the total electric charge (through G_E). The nucleon charge must be counted in the same way as in the vacuum, which leads to the requirement $E_E(M^2, \mathbf{Q}^2) = 1$ at $M = \mathbf{Q}^2 = 0$ for the enhancement factor of the nucleon electric Sachs form factor. Since the in-medium behavior of vector mesons does not depend on their origin (emission from nucleons or nucleon resonances), the constraints to the diagonal and the transition form factors must be identical. Hence, in the soft-dilepton limit, the coherence must be restored.

Equation (21) is the leading term when the density approaches zero. The condition for a fully decoherent scattering of particles propagating through a medium is the dilute gas limit. It means that sequential scattering processes are statistically independent. In terms of a scattering length, the dilute gas limit corresponds to the requirement that no additional scattering centers appear inside the wave zone of the scattered particle. In the present case this area can be estimated by a sphere of radius r, which is of the order of the meson wave length, $r \sim \lambda$. In the low-density limit this condition is satisfied, and Eq. (21) is applicable.

In the following, we intend to derive a modified expression for the collision length, which describes *qualitatively* also the intermediate and high density regime and provides the restoration of coherence in the soft-dilepton limit. The scattering has a coherent character if many scattering centers appear on the scale of the particle's wavelength λ. For a coherent scattering process on a cluster which consists of Z individual scattering centers, the cross section is given by

$$\sigma_Z \sim Z^2 \sigma, \tag{25}$$

where σ is the cross section for a single scattering center ($Z = 1$). If one assumes—as usually done—that the scattering centers are homogeneously distributed according to the density ρ_B, the probability to find a cluster with Z scattering centers inside a volume V is given by the Poisson distribution

$$P_Z = \frac{\alpha^Z}{Z!} e^{-\alpha}. \tag{26}$$

Here $\alpha = \rho_B V$ is the average number of scattering centers in the volume V. Coherent scattering takes place on clusters inside a sphere of radius $r \sim \lambda$. The average cross section for the scattering on clusters equals

$$\sigma_{\text{clus}} \sim \sigma \sum_{Z=0}^{+\infty} Z^2 \frac{\alpha^Z}{Z!} e^{-\alpha} = \sigma \alpha (1 + \alpha). \tag{27}$$

The average number of scattering centers inside a single cluster is

$$\bar{Z} = \sum_{Z=0}^{+\infty} Z \frac{\alpha^Z}{Z!} e^{-\alpha} = \alpha. \tag{28}$$

The ratio between Eqs. (27) and (28) now provides the effective cross section for the scattering on a single scattering center:

$$\sigma_{\text{eff}} \sim \sigma (1 + \alpha). \tag{29}$$

In the case of decoherent scattering, the above arguments lead to the relations $\sigma_Z \sim Z \sigma$, $\sigma_{\text{clus}} \sim \sigma \alpha$, and $\sigma_{\text{eff}} \sim \sigma$.

In relativistic heavy ion reactions the masses and momenta which occur in hadronic scattering processes are usually large, and thus quantum interference effects do not play a significant role. But here we are interested in the soft limit of the vector meson propagation, and thus one has to account for quantum effects. From scattering theory one knows that

the radiation takes place if the asymptotic regime $\sim 1/r$ starts for the wave function of the scattered particle outside the wave zone. When scattered on a cluster, the incident particle can hit new scattering centers inside the wave zone, and in this case radiation is assumed not to be formed. This means that a discrete scattering process can only take place on those clusters which leave the wave zone of the scattered particle unblocked, i.e., free from new scattering centers. The probability to find such a configuration can be estimated by the Poisson law:

$$P_{\text{unblocked}} \sim e^{-\alpha}. \tag{30}$$

The value of $P_{\text{unblocked}}$ is the probability that no additional scattering centers exist inside the wave zone, which we consider to be simply a region around the scattering cluster of the same volume V. The collision probability is then proportional to the effective cross section σ_{eff} multiplied by the probability $P_{\text{unblocked}}$ for an unblocked wave zone. The modification of Eq. (21) is now straightforward:

$$L_C \sim \frac{e^{\alpha}}{\rho_B \sigma (1+\alpha)}, \tag{31}$$

with $\alpha = \rho_B (4\pi/3)\lambda^3$. Expression (31) has finally the desired features. In the low density limit one obtains $\alpha \to 0$, and thus expression (21) is recovered. In the long wave limit $\alpha \to \infty$, $L_C \to \infty$, $w \to 1$, and so the full coherence is restored. Note that the function $e^{\alpha}/(1+\alpha)$ is a monotonously increasing function.

The wavelength λ is inverse proportional to the center-of-mass momentum of the vector meson and the cluster,

$$\frac{1}{\lambda} \sim p^*(\sqrt{s}, M, \bar{m}) \tag{32}$$

where $\bar{m}^2 = (\Sigma_{i=1}^Z p_i)^2$, p_i are the four-momenta of the nucleons in the cluster. Here $s = (P + \Sigma_{i=1}^Z p_i)^2$ and P is the vector meson momentum, $P^2 = M^2$. In the local rest frame of the cluster, i.e., the center-of-mass frame of its constituents, the vector meson momentum is given by

$$p^*(\sqrt{s}, M, \bar{m}) = \frac{\bar{m}}{\sqrt{s}} |\mathbf{Q}_{\text{clus}}|, \tag{33}$$

where $s = M^2 + 2P_0\bar{m} + \bar{m}^2$ and $P_0 = \sqrt{M^2 + \mathbf{Q}_{\text{clus}}^2}$. In order to obtain an infinite wavelength $\lambda = \infty$, one has to require that the vector meson momentum vanishes simultaneously in the rest frames of all clusters, $\mathbf{Q}_{\text{clus}}^2 = 0$. This is, however, only possible if the condition $M = \mathbf{Q}^2 = 0$ is fulfilled. Thus, at finite density a full restoration of the coherence can only take place for $M = \mathbf{Q}^2 = 0$. This condition appears quite reasonable, since a vector meson at rest with $M \neq 0$ and $\mathbf{Q}^2 = 0$ can still collide with the surrounding nucleons due to the Fermi motion and/or motion caused by a finite temperature.

It is interesting to note that $L_C \to \infty$ both at $\rho_B \to 0$ and $\rho_B \to \infty$. This implies the full restoration of coherence at finite λ for both small and infinite densities. For large clusters

$(Z \to \infty)$ $\bar{m} \sim Zm$ becomes dominant over M and P_0, and so $p^*(\sqrt{s}, M, \bar{m}) \to |\mathbf{Q}_{\text{clus}}|$. The c.m. velocity $\mathbf{v}_{\text{clus}}$ of a large cluster relative to the matter rest frame vanishes as $\mathbf{v}_{\text{clus}}^2 \sim 1/Z$. It follows that $|\mathbf{Q}_{\text{clus}}| \to |\mathbf{Q}|$ and $1/\lambda \to |\mathbf{Q}|$. For a single scattering center, $\bar{m} = m$, and the wavelength λ is determined by the momentum $p^*(\sqrt{s}, M, m)$ averaged over the nucleon velocity distribution in the matter.

In deriving Eq. (31), we neglected the dependence of λ on Z. Although very qualitative, Eq. (31) provides the desired behavior of the decoherence factors in the soft-dilepton limit. It leads to $L_C \to \infty$, $w_k \to 1$, $E_T^{(\pm)}(M^2, \mathbf{Q}^2) \to 1$ at $\lambda \to \infty$ $(M, \mathbf{Q}^2 \to 0)$, so that vector mesons with $M, \mathbf{Q}^2 \to 0$ propagate in a dense medium coherently. The decoherence becomes generally weaker with increasing λ.

The requirement of a restoration of coherence in the soft-dilepton limit follows directly from charge conservation. It is of principle importance but has no immediate practical implications for the description of experimental spectra. The experimental filters cut the dilepton spectra at low values of M, and thus this limit is presently not accessible. We do not discuss here possible effects of the mass dependence of the decay time through the equation $T_D = 1/\Gamma(M^2)$ or through Eq. (41). Note also that the meaning of the cross section entering the collision length L_C becomes unclear when M falls below the two-pion threshold (for ρ mesons), so the above discussion is restricted to the case of massless pions.

IV. THE QMD TRANSPORT MODEL

Heavy-ion reactions are described within the framework of the quantum molecular dynamics (QMD) transport model [35]. We extended our QMD transport code [36] in order to include all nuclear resonances with masses below 2 GeV. These are altogether 11 N^* and 10 Δ resonances. The corresponding masses and decay widths are listed in Tables III and IV. For the description of the dilepton production through baryonic resonances, respectively, the ρ and ω production in NN and πN reactions, only the well established (4*) resonances listed by the PDG [48] are taken into account. This corresponds to the same set of resonances which was used in Refs. [21,34], for the description of vector meson and dilepton production. The Γ_{tot}, and the $N\rho$ and $N\omega$ widths given in brackets as well as the decay widths of the other decay channels are taken from Ref. [47] and used for the reaction dynamics.

As in the previous calculations [36], we take the isospin dependent production cross sections $\sigma^{NN \to NR}$ for the $\Delta(1232)$ and the $N^*(1440)$ resonances from Ref. [64]. These cross sections were determined within the framework of a one-boson-exchange model. For the higher-lying resonances, parametrizations for the production cross section are taken from different sources [47,46]. The following types of baryon-baryon collisions are included: all elastic channels, reactions of the type $NN \to NN^*$, $NN \to N\Delta^*$, $NN \to \Delta_{1232}N^*$, $NN \to \Delta_{1232}\Delta^*$; and $NR \to NR'$, where Δ^* denotes all higher lying Δ resonances. Elastic scattering is considered on the same footing for all the particles involved. Matrix elements for elastic reactions are assumed to be the

same for nucleons and nucleonic resonances. Thus elastic NR and RR cross sections are determined from the elastic pp or np cross sections, depending on the total charge. Inelastic collisions are considered according to the expression [47]

$$\sigma_{1,2\rightarrow3,4}\sim\frac{\langle p_f\rangle}{p_i s}|\mathcal{M}(m_3,m_4)|^2, \tag{34}$$

p_i and $\langle p_f\rangle$ are the momenta of incoming and outgoing particles in the center-of-mass frame. In the case that final states are resonances, the phase space has to be averaged over the corresponding spectral function,

$$\langle p_f\rangle=\int p(\sqrt{s},m_N,\mu)dW_{R'}(\mu), \tag{35}$$

with $dW_{R'}$ given by the corresponding Breit-Wigner distribution (10). In the general case that both the final states in Eq. (34) are resonances, the averaging of p_f is performed over both resonances,

$$\langle p_f\rangle=\int p(\sqrt{s},\mu,\mu')dW_R(\mu)dW_{R'}(\mu'). \tag{36}$$

The integrations are performed over kinematically defined limits. $\mathcal{M}$ in Eq. (34) is the matrix element of the cross section, and the proportionality sign accounts for possible overall (iso)spin coefficients. For most of the cases we use expressions for the matrix elements from Ref. [47]. However, parametrizations of the matrix elements are given in Ref. [46], and we make use of these expressions. This is, in particular, the case for reactions where resonances contribute to the dilepton yield (see Tables III and IV). For example, the cross section for the reactions $NR\rightarrow NR'$ is determined from the known channels $NN\rightarrow NR$ and $NN\rightarrow NR'$ by

$$\sigma_{NR\rightarrow NR'}=I\frac{0.5(|\mathcal{M}_{NN\rightarrow NR}|^2+|\mathcal{M}_{NN\rightarrow NR'}|^2)2(2J_{R'}+1)}{16\pi p_i s}$$

$$\times\langle p_f\rangle. \tag{37}$$

In Eq. (37), I is an isospin coefficient, depending on the resonances' types, and $J_{R'}$ denotes the spin of R'.

For all resonances we use mass-dependent widths in expressions (37) and (36), namely

$$\Gamma(\mu)=\Gamma_R\left(\frac{p}{p_r}\right)^3\left(\frac{p_r^2+\delta^2}{p^2+\delta^2}\right)^2. \tag{38}$$

In Eq. (38) p and p_r are the c.m. momenta of the pion in the resonance rest frame evaluated at the running and the resonance pole mass, respectively. $\delta=0.3$ is chosen for the Δ_{1232} and $\delta=\sqrt{(m_R-m_N-m_\pi)^2+\Gamma^2/4}$ for the rest of the resonances. The inclusive π^-p and π^+p cross sections are shown in Fig. 11. The fit to the data including the sum over all resonances is of similar quality as in Refs. [46,47] and reproduces the absorption cross section up to pion laboratory momenta of 1–1.5 GeV. At higher energies string excitations start to play a role [47].
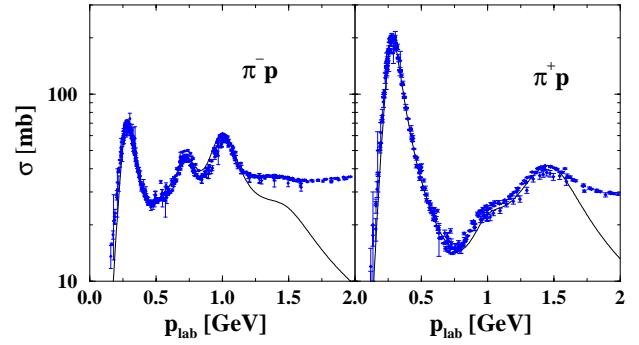

FIG. 11. Inclusive π^-p and π^+p cross sections obtained by the sum over all resonances which are taken into account in the present description (see Tables III and IV). Data are taken from Ref. [48].

Backward reactions, e.g., $NR\rightarrow NN$, are treated by the detailed balance

$$\sigma_{3,4\rightarrow1,2}\sim\frac{|p_{1,2}|^2}{|p_{3,4}|^2}\sigma_{1,2\rightarrow3,4}, \tag{39}$$

where the proportionality sign is due to overall (iso)spin factors. The expressions for the momenta of incoming (outgoing) particles are calculated according to Eqs. (37) and (36), respectively.

Pion-baryon collisions are standardly treated as two-stage processes, i.e., first the pion is absorbed by a nucleon or a baryonic resonance forming a new resonance state with subsequent decay. The pion absorption by nucleons is treated in the standard way [36,46,47], and the pion absorption by resonances is proportional to the partial decay width of the reverse process [46],

$$\sigma_{\pi R\rightarrow R'}=\frac{2J_{R'}+1}{(2S_a+1)(2S_b+1)}\frac{4\pi}{p_i^2}\frac{s(\Gamma_{R'\rightarrow R\pi})^2}{(s-m_{R'}^2)^2+s\Gamma_{R'}^2}. \tag{40}$$

The decay of baryonic resonances is treated as proposed in Refs. [65–67], i.e., the resonance life time is given by the spectral function

$$\tau_R(\mu)=4\pi\mu\frac{dW_R(\mu)}{d\mu^2}. \tag{41}$$

Here we use constant widths when considering resonance decays. The decay channels which are taken into account are listed in Tables III and IV, together with their corresponding branching ratios. For the mass systems under consideration pion multiplicities are reasonably well reproduced by the present description. For example, inclusive π^+ cross sections in C+C reactions were recently measured by the KaoS Collaboration [68], and the experimental results can be reproduced by the present description within error bars.

Concerning η, the fit of Ref. [45] is in good agreement with the exclusive $pp\rightarrow pp\eta$ production data from COSY [59] around threshold. Thus in this case we apply the cross section from Ref. [45] and neglect the η production through
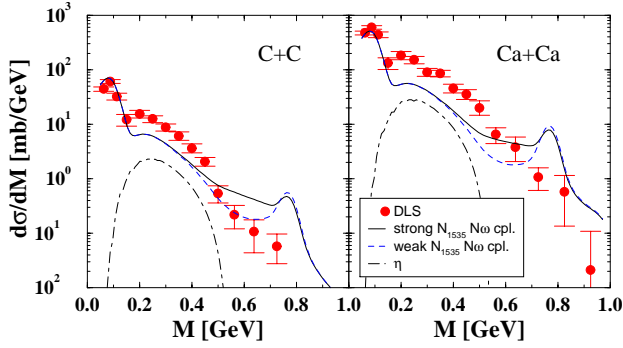
FIG. 12. The dilepton spectrum in C+C and Ca+Ca reactions is compared to the DLS data [14]. The calculations are performed with a strong, respectively a weak $N^*(1535)$-$N\omega$ coupling.

resonances. As a consistency check we compared the direct η production by the process $NN \rightarrow NN\eta$ to that of $NN \rightarrow RN \rightarrow NN\eta$, and found that the two production mechanisms lead to almost identical η yields in heavy ion reactions. However, to avoid double counting only one of the channels should be included. In line with experimental data [69] for η, an isospin factor of

$$\sigma(pn \rightarrow pn\,\eta) = 6.5\,\sigma(pp \rightarrow pp\,\eta) \tag{42}$$

is assumed.

V. DILEPTON PRODUCTION IN HEAVY-ION REACTIONS

A. Standard treatment

With this input QMD transport calculations for C+C and Ca+Ca reactions at 1.04A GeV are performed. First we discuss the results obtained without any additional medium effects concerning the dilepton production. For the nuclear mean field a soft momentum dependent Skyrme force ($K = 200$ MeV) is used [35], which provides also a good description of the subthreshold K^+ production in the considered energy range [70]. The reactions are treated as minimal bias collisions with maximal impact parameters $b_{max} = 5(8)$ fm for C+C (Ca+Ca).

In Fig. 12 the results are compared to the DLS data. The acceptance filter functions provided by the DLS Collaboration are applied, and the results are smeared over the experimental resolution of $\Delta M = 35$ MeV. The calculations are performed within the two scenarios discussed in Sec. II, namely, a strong $N^*(1535)$-$N\omega$ coupling as implied by the original fit to the available photoproduction data [34] and a weaker coupling which can be enforced by a different choice of input parameters. In the first case strong off-shell ω contributions appear, which are also visible in the dilepton spectrum at invariant masses below the ω peak. In the mass region between 0.4–0.8 GeV, the two scenarios yield significantly different results. The rest of the spectrum is practically identical, except the height of the ω peak itself. As discussed in connection with the elementary cross sections, the ω contribution from the $N^*(1535)$ is suppressed at the ω pole in the strong coupling scenario, and thus the total ω peak is slightly lower. The comparison of the transport

calculations with the DLS data is here not completely conclusive: The lighter C+C system would favor the weak $N^*(1535)$-$N\omega$ coupling scenario whereas the Ca+Ca reactions are better described by the strong coupling.

In the low mass region ($M = 0.1$–0.5 GeV) we observe an underestimation of the DLS spectra by a factor of 2–3. Thus in the present approach the underestimation of the DLS data is somewhat smaller than observed in the previous works of Refs. [15,12]. One reason for this is a larger η contribution, which is probably due to the isospin factor of 6.5 for the $np \rightarrow np\,\eta$ channel (compared to a factor of 2.5 used in Refs. [12,28]). Other differences to the previous treatments [15,12] are the following: In Ref. [12] the vector meson production was described by parametrizations of the NN and πN production channels, while in the present approach these reactions run solely over the excitation of intermediate nucleon resonances. In Refs. [15,12] only the $\Delta(1232) \rightarrow Ne^+e^-$ Dalitz decay has explicitly been included. In addition, the decays of the nucleon resonances into vector mesons were treated till recently in the nonrelativistic approximation [28,24], and usually only one transition form factor was taken into account. From counting the independent helicity amplitudes it is clear that a phenomenologically complete treatment requires three transition form factors for spin $J \geq 3/2$ nucleon resonances and two transition form factors for spin-1/2 resonances. Earlier attempts to derive a complete phenomenological expression for the dilepton decay of the $\Delta(1232)$ were not successful (for a discussion see Ref. [32]). Despite the details which differ in the various transport calculations (we included significantly more decay channels and apply an improved description of the baryonic resonance decays) the present results confirm qualitatively the underestimation of the DLS data at invariant masses below the ρ/ω peak [15,12].

A deviation to the results of Refs. [15,12] and appears in the vicinity of the ω peak. Even after averaging over the experimental resolution, the present results show a clear peak structure around 0.8 GeV, which is absent in Refs. [15,12]. However, in Ref. [12] absorptive channels (e.g., $N\omega \rightarrow N\pi$ [71]) have been included, which lead automatically to a collisional broadening of the in-medium vector meson width. Such a collision broadening is not included in the results shown in Fig. 12, but will be separately discussed in the following section. With respect to the UrQMD calculations of Ref. [15] our approach is in principle similar, because vector mesons are produced through the excitation of nuclear resonances. However, in Ref. [15] the naive VMD was applied to treat the mesonic decays and the treatment is more qualitative, i.e., couplings were not particularly adjusted in order to describe ρ and ω cross section, as it was done in Refs. [33,34]. For example, in Ref. [15] only the $N^*(1900) \rightarrow N\omega$ decay mode was taken into account, which leads presumably to a significant underestimation of the $NN \rightarrow NN\omega$ cross section.

The contributions of the various nuclear resonances are displayed in Fig. 13 for the Ca+Ca reaction. Here the theoretical results are not averaged according to the experimental resolution, but the DLS filter is applied and the data are also shown in order to guide the eye. The contributions from the
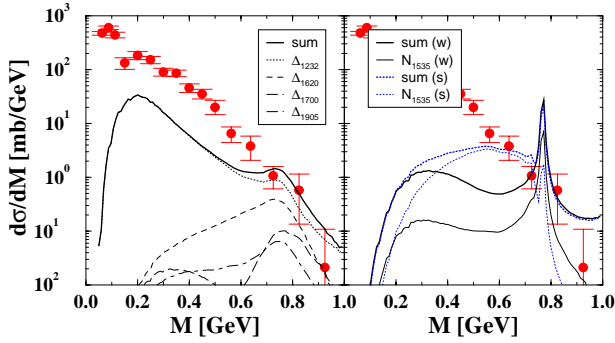
FIG. 13. Contributions of various nuclear resonances to the dilepton spectra in Ca+Ca reactions at 1.04A GeV. Left: contributions from Δ decays. Right: The total contribution from N^* decays and that of the $N^*(1535)$ are shown for the two scenarios of a strong/weak (s/w) $N^*(1535)$-$N\omega$ coupling. The DLS data [14] are shown in order to guide the eye.

FIG. 14. Contributions of various N^* resonances to the dilepton spectra in Ca+Ca reactions at 1.04A GeV.

Δ resonances which run exclusively over ρ decays are dominated by the $\Delta(1232)$. However, in the vicinity of the ρ peak, the $\Delta(1620)$ gives an almost comparable contribution. The $\Delta(1700)$ and $\Delta(1905)$ give only minor contributions. The N^* resonances which contribute both, via ρ and ω decays, are in particular important at invariant masses around and slightly below the ρ/ω peak. Before smearing over the experimental resolution, the ω peak is clearly visible. As discussed in Sec. II in connection with the elementary production cross sections, the $N^*(1535)$ plays a crucial role in our treatment. Therefore we display the contribution from this resonance separately for the two scenarios of a strong and a weak $N^*(1535)$-$N\omega$ coupling. The first case (strong coupling) results in a smaller on-shell ω cross section, which is reflected in a lower ω peak in the dilepton spectrum. The reason for the smaller on-shell value is a suppression of the ω strength from this resonance just at the ω pole [34]. However, this scenario leads to a strong background contribution which is experimentally not accessible in ω production measurements but is clearly reflected in the enhanced dilepton spectrum below the ω pole. Compared to the weak coupling scenario, the dilepton yield from $N^*(1535)$ is enhanced by almost one order of magnitude in this mass region. In the weak coupling scenario, on the other hand, the $N^*(1535)$ plays only a minor role in this kinematical region.

The contributions of the other N^* resonances are shown in Fig. 14. In the low mass region the most important one is the $N^*(1520)$, which has a strong ρ decay mode [33]. At the ω peak the $N^*(1520)$ and the $N^*(1680)$ dominate. Similar relative yields are obtained in C+C reactions.

In summary, one can conclude that the theoretical calculations without medium effects show, in two distinct kinematical areas, clear deviations from experiment: the low mass region between $M=0.1$ and 0.5 GeV is underestimated, while the contribution at the ω (and ρ) peak is strongly overestimated. We also investigated the contributions from $\pi^+\pi^-$ annihilation. In our calculations the influence of this channel is significantly smaller than that in Ref. [12], and does not play an important role.
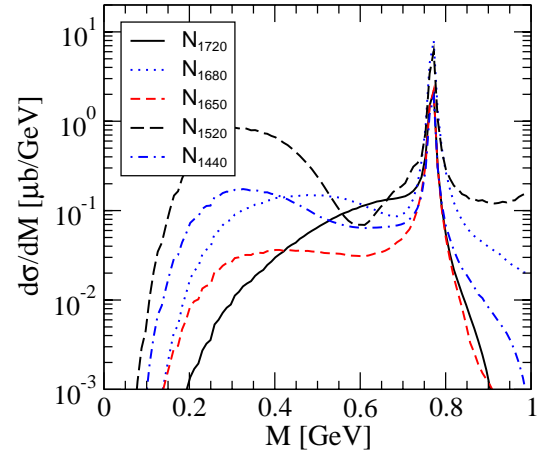
B. ρ and ω meson in-medium widths

In previous studies, in-medium spectral functions of the ρ and ω mesons were implemented into heavy-ion codes *ab initio* [12]. At intermediate energies, the sensitivity of the dilepton spectra on the in-medium ρ-meson broadening is less pronounced as compared to the ω meson. Estimates for the collision broadening of the ρ in hadronic matter, i.e., dense nuclear matter or a hot pion gas, predict a collision width which is of the magnitude of the vacuum ρ width. For ω, on the other hand, the vacuum width is only 8.4 MeV, whereas in the medium it is expected to be more than one order of magnitude larger. However, the possibility of a strong in-medium modification of the ω meson has not attracted much attention in previous studies. The reason is probably due to the fact that the direct information on the ω-meson channels from resonance decays, available through the multichannel πN scattering analysis, is quite restricted. The present model provides an unified description of the photoproduction and electroproduction data, and of the vector meson and dilepton decays of the nucleon resonances. It also provides a reasonable description of the vector meson and the dilepton production in elementary reactions ($p+p,p+d$) in the BEVALAC energy range. However, when applied to $A+A$ reactions, the model leads to a very strong overestimation of the dilepton yield around the ω peak, which suggests significant medium modifications of the ω contribution. At low energies, the vector meson production occurs due to decays of nucleon resonances. The in-medium broadening of vector mesons can be understood within the framework of the resonance model. It has qualitatively two major consequences: (1) an increase of the nucleon resonance decay widths $R\rightarrow NV$, (2) a decrease of the dilepton branchings $V\rightarrow e^+e^-$ due to the enhanced total vector meson widths.

These two effects are of opposite signs and can be completely described in terms of Eqs. (3)–(6) through appropriate modifications of the vector meson propagators entering into the $RN\gamma$ transition form factors $G_T(M^2)$. Within the eVMD framework, it is sufficient to increase the total widths

of the vector mesons. In a less formal way, the effect can be explained as follows. The differential branching

$$dB(\mu,M)^{R\to NV} = \frac{d\Gamma^R_{NV}(\mu,M)}{\Gamma_R(\mu)} \qquad (43)$$

becomes usually larger with an increasing V meson width, which is due to the subthreshold character of the vector meson production through the light nucleon resonances. The dilepton branching of the nucleon resonances,

$$B(\mu)^{R\to Ne^+e^-} \sim B(\mu)^{R\to NV} \frac{\Gamma_{V\to e^+e^-}}{\Gamma^{tot}_V}, \qquad (44)$$

is, on the other hand, inversely proportional to the total vector meson width Γ^{tot}_V. Hence, an increase of the total width results in a decrease of the dilepton production rate. This effect is particularly strong for ω since the in-medium ω width is expected to be more than one order of magnitude greater than in the vacuum [6]. Although the estimates of Ref. [6] were based on the standard VMD model which is contradictive with respect to the description of both, the RNV and $RN\gamma$ branchings [21,24,25], the qualitative conclusions concerning the magnitude of the in-medium ω broadening should be valid. A relatively large ω collision width is not too surprising. According to the SU(3) symmetry the ω coupling to nucleons is three times greater than the ρ coupling. One can therefore expect that at identical kinematical conditions the $N\omega$ cross section will be greater than the $N\rho$ cross section. Since the collision widths are proportional to the cross sections, the same conclusion holds for the collision widths. The ω contribution is extremely sensitive to the reaction conditions in the course of the heavy-ion collisions. While the increase of the total branching $B(\mu)^{R\to NV}$ depends on kinematical details, one can expect that the suppression of the ω contribution due the enhanced total width Γ^{tot}_ω is a one order of magnitude effect.

In the standard approach without additional medium effects, Fig. 12, both possibilities, i.e., the strong and the weak $N^*(1535)$-$N\omega$ decay modes, lead to a significant overestimation of the DLS data in the vicinity of the ω peak. An empirical way to investigate the influence of the collisional broadening is to assume in a first step average in-medium values for $\Gamma^{tot}_{\rho/\omega}$, and to compare the corresponding results to the experiment. In Figs. 15 and 16 this is done for the Ca+Ca reaction. The QMD results are shown for two values of the in-medium ρ width, i.e., the vacuum value of 150 MeV and $\Gamma^{tot}_\rho = 300$ MeV.

The latter assumes an additional collision width of $\Gamma^{coll}_\rho = 150$ MeV, which agrees with the estimates of Refs. [4–7]. In both cases the ω width is varied between $\Gamma^{tot}_\omega = 8.4$, 50, 100, 200, and 400 MeV. As already mentioned, the in-medium ω broadening is less studied. Thus we cover the possible range of in-medium values by the above parameter set.

First of all, it is important to realize that the region which is sensitive to in-medium modifications of the meson widths is distinct from the mass interval between 0.2 and 0.6 GeV
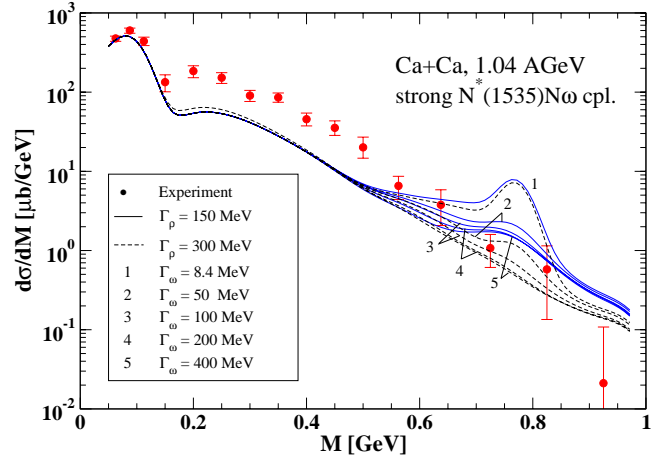

FIG. 15. Dilepton spectra in Ca+Ca collisions at 1.04*A* GeV for different values of the in-medium ρ and ω widths. The solid curves correspond to calculations where the ρ width is kept at its vacuum value of 150 MeV (no collision broadening). The dashed curves correspond to a total ρ width of 300 MeV. In both cases the ω width is varied between $\Gamma^{tot}_\omega = 8.4$–400 MeV. The results are obtained with the strong $N^*(1535)$-$N\omega$ coupling.

where the DLS puzzle is observed. This means that the problem to extract in-medium vector meson widths is isolated from the difficulties concerning the theoretical interpretation of the dilepton spectra below the ρ/ω peak. As expected, the dilepton spectra in the vicinity of the ρ/ω peak react very sensitive on modifications of the in-medium width. The reproduction of the DLS data requires an in-medium ω width which lies above 50 MeV for both strong and weak couplings. The best fits are obtained with $\Gamma^{tot}_\rho = 300$ MeV and $\Gamma^{tot}_\omega = 100$–300 MeV. With these values we reproduce in the strong $N^*(1535)$-$N\omega$ coupling scenario the DLS data points around and 100 MeV below the ρ/ω peak within error bars. In the weak coupling scenario the DLS data are still slightly underestimated below the peak. However, the situation is not completely conclusive if one considers also the C+C system, Fig. 17, where the strong coupling lies slightly above
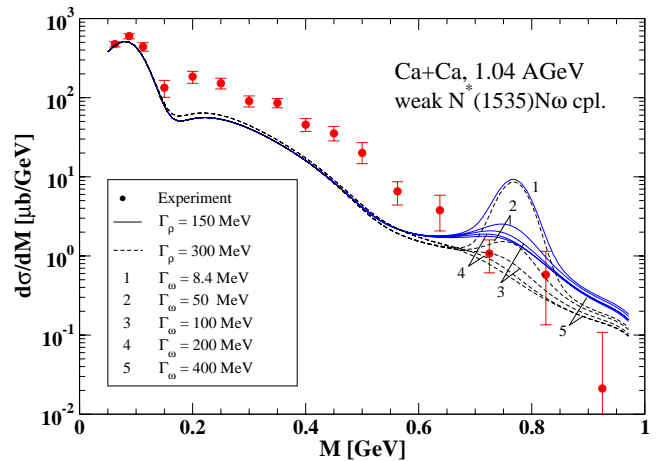

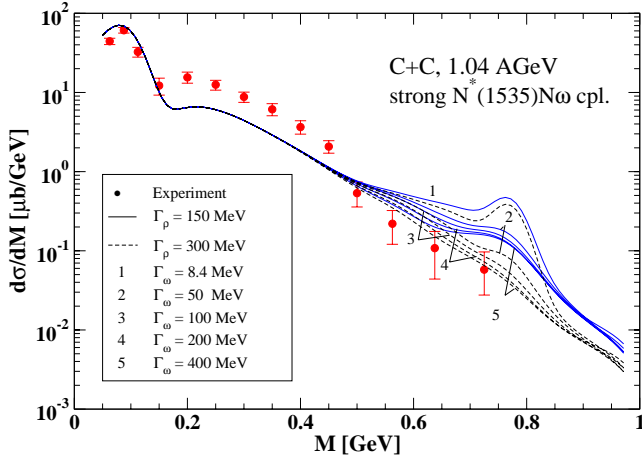FIG. 16. Same as Fig. 15, but with weak $N^*(1535)$-$N\omega$ coupling.

FIG. 17. Dilepton spectra in C+C collisions at 1.04*A* GeV for different values of the in-medium ρ and ω widths. The solid curves correspond calculations where the ρ width is kept at its vacuum value of 150 MeV (no collision broadening). The dashed curves correspond to a total ρ width of 300 MeV. In both cases the ω width is varied in the range $\Gamma_\omega^{tot}=8.4$–400 MeV. The results are obtained with the strong $N^*(1535)$-$N\omega$ coupling.

error bars even with in-medium meson widths. Definite conclusions on the $N^*(1535)$-$N\omega$ mode from dilepton yields in heavy-ion reactions require more precise data which will be provided by the HADES Collaboration [72]. The present estimates can be interpreted as empirical values which are directly extracted from the experiment. The strength of the ω broadening and the theoretical motivation through Eq. (44) provide confidence for these estimates.

If the average widths are fixed one can (on the other hand) extract an average cross section from the collision broadening condition $\Gamma_{VN}^{coll}=\langle\rho_B\rangle v \gamma \sigma_{VN}$. The average nuclear density at the vector meson production, respectively, at the decay of the corresponding nuclear resonances R, is in minimal bias 1*A* GeV Ca+Ca reactions about 1.5 times the saturation density, i.e., $\langle\rho_B\rangle_{Ca+Ca}=0.24$ fm^{-3} and slightly less for C+C ($\langle\rho_B\rangle_{C+C}=0.20$ fm^{-3}). If one assumes now that the vector mesons are produced in an isotropic fireball with a temperature of $T\simeq80$ MeV, the extracted collisional width corresponds to an average ρN cross section of about $\sigma_{\rho N}\simeq30$ mb and $\sigma_{\omega N}\simeq50$ mb for ω ($\Gamma_\omega^{tot}=200$ MeV) [73].

C. Decoherence

The collision broadening of the vector mesons discussed above is most pronounced at invariant masses close to ρ and ω pole masses. A possible decoherence between the intermediate mesonic states in the resonance decays, in contrast, affects the dilepton spectrum preferentially below the ρ/ω peak (see Sec. III). The values which have already been extracted for the collision broadening of the vector mesons will therefore not significantly be changed when decoherence effects are additionally taken into account. Hence, we consider the values $\Gamma_\rho^{coll}=150$ MeV and $\Gamma_\omega^{coll}=100$–300 MeV already as final estimates, which must not be iterated.
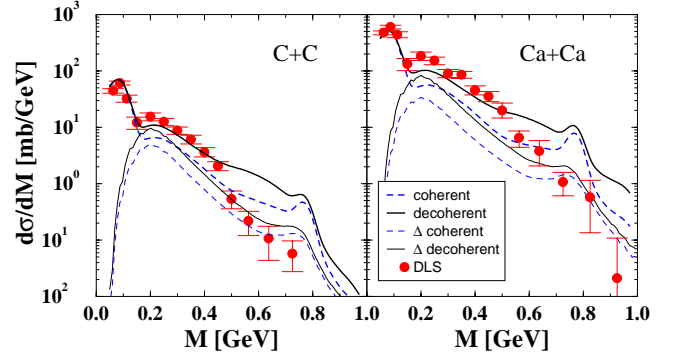

FIG. 18. Influence of a totally decoherent dilepton emission in C+C and Ca+Ca reactions. The contributions from the Δ resonances are in both cases shown separately.

The decoherence effect is treated as described in Sec. III. The collision broadening and the collision length are related through the equations

$$e^{-l_C/L_C}=e^{-vt/L_C}=e^{-\Gamma_V^{coll}t/\gamma}. \tag{45}$$

Expression (45) provides the probability that a meson V travels after its creation the length l_C through the medium without being scattered by the surrounding hadrons. In Eq. (45), v is velocity and γ is the Lorentz factor. The collision length and width are thus related by

$$v/L_C=\Gamma_V^{coll}/\gamma. \tag{46}$$

The collision length for the mesons is given by Eq. (31). An effective cross sections σ_{VN} (which is related to the collision width) corresponds to Eq. (31), i.e., the factors $(1+\alpha)e^{-\alpha}$ in Eq. (31) are then effectively included. Since the collision widths are directly extracted from data, the ρ and ω collision lengths which are necessary in order to determine the probabilities for a coherent dilepton emission can be obtained from Eq. (46). The estimates of the collision lengths for radially excited vector mesons are thereby assumed to be the same as for the ground-state vector mesons. The vacuum widths of the radially excited mesons are larger than those of the ground state ρ and ω. As a consequence, the radially excited mesons show a tendency to decay coherently. The decoherence effect is most pronounced for the ground-state ω meson, since its vacuum width is particularly small. The ω meson decays in the medium almost fully decoherently, i.e., after its first collision with another hadron. This results in a modification of the $N^*\rightarrow Ne^+e^-$ decay rates of the $I=1/2$ resonances due to the destruction of the interference between the $I=0$ and $I=1$ transition form factors. Since for the considered reactions the matter is isospin symmetric, the breakup of the ρ-ω coherence does not result in a significant change of the dilepton spectra. In this case the isoscalar-isovector interference terms cancel on average. The major effect arises from the break up of the interference between the ω and its radial excitations.

In Fig. 18 the influence of the decoherent summation of the intermediate mesonic states in the transition form factors is shown for both, Ca+Ca and C+C reactions. To demon-
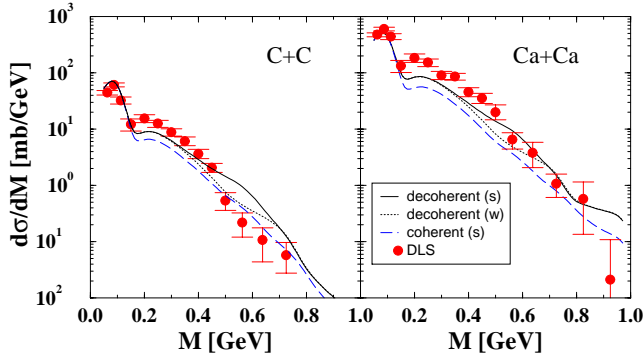
FIG. 19. Influence of the microscopically determined decoherent dilepton emission in C+C and Ca+Ca reactions. The calculations are performed with in-medium ρ and ω widths of 300 and 200 MeV, respectively. The strong (*s*) and weak (*w*) $N^*(1535)$-$N\omega$ couplings are used. For comparison also the coherent case (*s*) is shown.

strate the maximal possible effect we assume first total decoherence of all intermediate mesons. In this calculation no further medium effects are considered, i.e., the ρ/ω vacuum widths are used and the strong $N^*(1535)$-$N\omega$ coupling is applied (the corresponding coherent calculations are the same as in Fig. 12). A totally decoherent summation of the mesonic amplitudes in the resonance decays enhances the dilepton yield generally by about a factor of 2. In the low-mass region this enhancement is able to describe the DLS data. As can be seen from Fig. 18, this fact is due the enhancement of the Δ contributions by a factor of 2–3. However, also at larger invariant masses above 0.4 GeV the yield is enhanced, and the spectrum is now stronger overestimated than in the coherent case. In the mass region between 0.4 and 0.8 GeV, the N^* resonances give the major contribution to the yield. One has to keep in mind that the enhancement arises from the sum over the various Δ and N^* resonances and the interplay between the corresponding electric, magnetic, and Coulomb form factors. The enhancement is thus a complex function of the dilepton mass M. However, the scenario of a completely decoherent dilepton emission is rather unrealistic.

In a realistic calculation shown in Fig. 19, the probabilities for coherent/decoherent dilepton emission are determined microscopically as outlined above, i.e., by the use of Eqs. (22)–(24), and (45). These realistic calculations are performed using the "optimal" values for the in-medium widths of $\Gamma_\rho^{coll} = 150, \Gamma_\omega^{coll} = 200$ MeV. The low-mass dilepton yield is now enhanced by about 50% by the decoherence effect which is, however, still too small to describe the DLS data. The interplay between the two in-medium effects, i.e., the collisional broadening and the decoherent dilepton emission is more complex. Decoherence also leads to an enhancement of the dilepton yield in the mass region between 0.4 and 0.7 GeV. Since the main decoherence effect occurs through the broken interference of ω with its excited states, it is most pronounced in the dilepton contribution which stems from the N^* resonance decays. This explains the difference between the two calculations assuming a strong/weak $N^*(1535)$-$N\omega$ coupling in the mass range where possible off-shell ω contributions are now enhanced (strong cou-

pling). However, definite conclusions on the strength of the $N^*(1535)N\omega$ coupling are still difficult to make at the present data situation. For the strong coupling, the Ca+Ca system is in agreement within error bars with the DLS data whereas in the lighter C+C system the data are now overestimated and would favor the weak coupling. In both cases the agreement with the data is significantly improved in the low-mass region. However, the considered decoherence effects are not completely sufficient in order to solve the DLS puzzle. The reason is that the microscopic determination of the decoherence probability favors the breakup of the coherence between the ω and its excited states in the N^* decays rather than the breakup between ρ and its excited states in the Δ decays. The latter resonances are, however, those which contribute to most extent at low invariant masses.

VI. CONCLUSION

In the present work we provided a systematic description of vector meson and dilepton production in elementary NN and πN as well as in $A+A$ reactions. The reaction dynamics of the heavy-ion collisions is described by the QMD transport model which was extended for the inclusion of nucleon resonances with masses up to 2 GeV. The vector meson production in elementary reactions is described through excitations of nuclear resonances within the framework of an extended VMD model. The model parameters were fixed utilizing electroproduction and photoproduction data as well as πN scattering analysis. Available data on the ρ and ω production in $p+p$ and $\pi+N$ reactions are well reproduced. The same holds for the dilepton production in elementary $p+p$ and $p+d$ reactions.

The situation becomes different turning to heavy-ion collisions: In C+C and Ca+Ca reactions we observe in two distinct kinematical regions significant deviations from the dilepton yields measured by the DLS Collaboration. At small invariant masses the experimental data are strongly underestimated, which confirms the observations made by other groups. Although accounting for the experimental resolution we observe further a clear structure of the ρ/ω peak, which is not present in the data. Both features imply the investigation of further medium effects.

The collisional broadening of the vector mesons suppresses the ρ/ω peak in the dilepton spectra. This allows to extract empirical values for the in-medium widths of the vector mesons. From the reproduction of the DLS data the following estimates for the collision widths $\Gamma_\rho^{coll} = 150$ MeV and $\Gamma_\omega^{coll} = 100$–300 MeV can be made. The in-medium values correspond to an average nuclear density of about $1.5\rho_0$. HADES will certainly help to constrain these values with higher precision.

The second medium effect discussed here concerns the problem of quantum interference. Semiclassical transport models like QMD do not generally account for interference effects, i.e., they propagate probabilities rather than amplitudes and assume that relative phases cancel the interference on average. However, interference effects can play an important role for the dilepton production. In the present model the decay of nuclear resonances, which is the dominant source

for the dilepton yield, requires the destructive interference of intermediate ρ and ω mesons with their excited states. The interference can at least partially be destroyed by the presence of the medium which leads to an enhancement of the corresponding dilepton yield. We proposed a scheme to treat the decoherence in the medium on a microscopic level. The account for decoherence improves the agreement with the DLS data in the low mass region. However, the magnitude of this effect is not sufficient to resolve the DLS puzzle completely.

ACKNOWLEDGMENTS

[1] G.E. Brown and M. Rho, Phys. Rev. Lett. **66**, 2720 (1991); Phys. Rep. **269**, 333 (1996).

[2] T. Hatsuda and S.H. Lee, Phys. Rev. C **46**, R34 (1992); Y. Koike, *ibid.* **51**, 1488 (1995); T. Hatsuda, S.H. Lee, and H. Shiomi, *ibid.* **52**, 3364 (1992); S. Leupold, *ibid.* **64**, 015202 (2001); S. Zschoke, O.P. Pavlenko, and B. Kämpfer, Eur. Phys. J. A **15**, 529 (2002).

[3] A. Bhattacharyya, S.K. Ghosh, and S.C. Phatak, Phys. Rev. C **60**, 044903 (1999).

[4] F. Klingl, N. Kaiser, and W. Weise, Nucl. Phys. **A624**, 527 (1997); F. Klingl and W. Weise, Eur. Phys. J. A **4**, 225 (1999).

[5] V.L. Eletsky and B.L. Ioffe, Phys. Rev. Lett. **78**, 1010 (1997).

[6] V.L. Eletsky, M. Belkasem, P.J. Ellis, and J.I. Kapusta, Phys. Rev. C **64**, 035202 (2001).

[7] L.A. Kondratyuk *et al.*, Phys. Rev. C **58**, 1078 (1998).

[8] G. Agakichiev *et al.*, Phys. Rev. Lett. **75**, 1272 (1995); A. Drees, Nucl. Phys. **A610**, 536c (1996).

[9] M. Masera, Nucl. Phys. **A590**, 93c (1995).

[10] W. Cassing, W. Ehehalt, and C.M. Ko, Phys. Lett. B **363**, 35 (1995); G.Q. Li, C.M. Ko, and G.E. Brown, Nucl. Phys. **A606**, 568 (1996); C.M. Hung and E.V. Shuryak, Phys. Rev. C **56**, 453 (1997).

[11] M. Urban, M. Buballa, R. Rapp, and J. Wambach, Nucl. Phys. **A641**, 433 (1998); **A673**, 357 (2000); R. Rapp and J. Wambach, Adv. Nucl. Phys. **25**, 1 (2000).

[12] E.L. Bratkovskaya, W. Cassing, R. Rapp, and J. Wambach, Nucl. Phys. **A634**, 168 (1998).

[13] R. Schneider and W. Weise, Eur. Phys. J. A **9**, 357 (2000).

[14] R.J. Porter *et al.*, DLS Collaboration, Phys. Rev. Lett. **79**, 1229 (1997).

[15] C. Ernst, S.A. Bass, M. Belkacem, H. Stocker, and W. Greiner, Phys. Rev. C **58**, 447 (1998).

[16] E.L. Bratkovskaya and C.M. Ko, Phys. Lett. B **445**, 265 (1999).

[17] T. Inoue and E. Oset, Nucl. Phys. **A710**, 354 (2002).

[18] K. Ozawa *et al.*, Phys. Rev. Lett. **86**, 5019 (2001).

[19] E.L. Bratkovskaya, Phys. Lett. B **529**, 26 (2002).

[20] A. Faessler, C. Fuchs, and M.I. Krivoruchenko, Phys. Rev. C **61**, 035206 (2000).

[21] A. Faessler, C. Fuchs, M.I. Krivoruchenko, and B.V. Martemianov, J. Phys. G **29**, 603 (2003).

[22] C. Song and V. Koch, Phys. Rev. C **54**, 1903 (1995).

[23] W. Cassing, E.L. Bratkovskaya, M. Effenberger, and U. Mosel, Nucl. Phys. **A653**, 301 (1999).

[24] B. Friman and H.J. Pirner, Nucl. Phys. **A617**, 496 (1997).

[25] M. Post and U. Mosel, Nucl. Phys. **A688**, 808 (2001).

[26] A.I. Titov and B. Kämpfer, Eur. Phys. J. A **12**, 217 (2001).

[27] M. Zetenyi and Gy. Wolf, nucl-th/0202047.

[28] E.L. Bratkovskaya, W. Cassing, and U. Mosel, Nucl. Phys. **A686**, 568 (2001).

[29] E.L. Bratkovskaya, Nucl. Phys. **A696**, 761 (2001); M. Effenberger, E.L. Bratkovskaya, W. Cassing, and U. Mosel, Phys. Rev. C **60**, 027601 (1999).

[30] M.F.M. Lutz, B. Friman, and M. Soyeur, Nucl. Phys. **A713**, 97 (2003).

[31] G. Penner, and U. Mosel, Phys. Rev. C **66**, 055211 (2002); **66**, 055212 (2002).

[32] M.I. Krivoruchenko and Amand Faessler, Phys. Rev. D **65**, 017502 (2002).

[33] M.I. Krivoruchenko, B.V. Martemyanov, A. Faessler, and C. Fuchs, Ann. Phys. (N.Y.) **296**, 299 (2002).

[34] C. Fuchs, M.I. Krivoruchenko, H. Yadav, A. Faessler, B.V. Martemyanov, and K. Shekther, Phys. Rev. C **67**, 025202 (2003).

[35] J. Aichelin, Phys. Rep. **202**, 233 (1991).

[36] V.S. Uma Maheswari, C. Fuchs, Amand Faessler, L. Sehn, D. Kosov, and Z. Wang, Nucl. Phys. **A628**, 669 (1998).

[37] N. Bianchi *et al.*, Phys. Lett. B **309**, 5 (1993); **325**, 333 (1994).

[38] L.A. Kondratyuk, M.I. Krivoruchenko, N. Bianchi, E.D. Sanctis, and V. Muccifora, Nucl. Phys. **A579**, 453 (1994).

[39] CMD-2 Collaboration, Phys. Lett. B **501**, 191 (2001); **503**, 237 (2001).

[40] A.I. Vainstein and V.I. Zakharov, Phys. Lett. **72B**, 368 (1978).

[41] L.G. Landsberg, Phys. Rep. **128**, 301 (1985).

[42] G. Hohler, E. Pietarinen, I. Sabba Stefanescu, F. Borkowski, G.G. Simon, V.H. Walther, and R.D. Wendling, Nucl. Phys. **B114**, 505 (1976).

[43] P. Mergell, U.G. Meissner, and D. Drechsel, Nucl. Phys. **A596**, 367 (1996).

[44] A. Sibirtsev, Nucl. Phys. **A604**, 455 (1996).

[45] A. Sibirtsev, W. Cassing, and U. Mosel, Z. Phys. A **358**, 357 (1997).

[46] S. Teis, W. Cassing, M. Effenberger, A. Hombach, U. Mosel, and Gy. Wolf, Z. Phys. A **356**, 421 (1997).

[47] S.A. Bass *et al.*, Prog. Part. Nucl. Phys. **41**, 225 (1998).

[48] Particle Data Group, Phys. Rev. D **54**, 1 (1996).

[49] F. Hibou *et al.*, Phys. Rev. Lett. **83**, 492 (1999).

[50] COSY-TOF Collaboration, Phys. Lett. B **522**, 16 (2001).

[51] F. Balestra *et al.*, DISTO Collaboration, Phys. Rev. C **63**, 024004 (2001).

[52] V. Flaminio *et al.*, CERN-HERA Report No. 84-10, 1984.

[53] A. Berthon, J. Mas, J.L. Narjoux, and P. Ladron de Guevara, Nucl. Phys. **B81**, 431 (1974); Y. Williamson *et al.*, Phys. Rev. Lett. **29**, 1353 (1972).

[54] W.K. Wilson *et al.*, DLS Collaboration, Phys. Rev. C **57**, 1865 (1998).

[55] A. Bussiere *et al.*, Nucl. Phys. **A365**, 349 (1981).

[56] H. Calen *et al.*, Phys. Rev. Lett. **79**, 2642 (1997); Phys. Rev. C **58**, 2667 (1998).

[57] E. Chiavassa *et al.*, Phys. Lett. B **337**, 192 (1994).

[58] F. Hibou *et al.*, Phys. Lett. B **438**, 41 (1998).

[59] J. Smyrski *et al.*, COSY-11 Collaboration, Phys. Lett. B **474**, 182 (2000).

[60] H. Calen *et al.*, Phys. Lett. B **366**, 39 (1996).

[61] E. Chiavassa *et al.*, Phys. Lett. B **322**, 270 (1994).

[62] A. Bergdolt *et al.*, Phys. Rev. D **48**, 2969 (1993).

[63] V.A. Matveev, R.M. Muradian, and A.N. Tavkhelidze, Lett. Nuovo Cimento **7**, 719 (1973); S.J. Brodsky and G.R. Farrar, Phys. Rev. Lett. **31**, 1153 (1973); Phys. Rev. D **11**, 1309 (1975).

[64] S. Huber and J. Aichelin, Nucl. Phys. **A573**, 587 (1994).

[65] P. Danielewicz and S. Pratt, Phys. Rev. C **53**, 249 (1966).

[66] J. Aichelin and C. Hartnack, in Proceedings to the 25th International Workshop on Gross Properties of Nuclei and Nuclear Excitations, Hirschegg, 1997, edited by H. Feldmeier *et al.*

[67] A.B. Larionov, M. Effenberger, S. Leupold, and U. Mosel, Phys. Rev. C **66**, 054604 (2002).

[68] C. Sturm *et al.*, KaoS Collaboration, Phys. Rev. Lett. **86**, 39 (2001).

[69] G. Faeldt and C. Wilkin, Nucl. Phys. **A587**, 769 (1995).

[70] C. Fuchs, Amand Faessler, E. Zabrodin, and Y.M. Zheng, Phys. Rev. Lett. **86**, 1974 (2001).

[71] E.L. Bratkovskaya and W. Cassing, Phys. Rep. **308**, 65 (1999).

[72] J. Friese, HADES Collaboration, Nucl. Phys. **A654**, 1017c (1999).

[73] As mentioned in the text, we used an averaging procedure with constant bin width $\sqrt{2}\sigma = 35$ MeV. If one applies a mass dependent smearing function as suggested by the DLS Collaboration, the contribution from the ω-peak can further be flattened. However, different smearing procedures do not affect the total dilepton yield and thus the problem of overestimation of the DLS spectra in the vicinity of the ω-peak remains. The conclusions on strong collision broadenings of the ρ- and ω-mesons which are required to reduce that yield are independent from the actual averaging procedure applied.